Journal of Electromagnetic Waves and Applications, Vol. 6, No. 2, 169–197, 1992

Variance of Phase Fluctuations of Waves Propagating through a Random Medium

N. C. Chu, J. A. Kong, H. A. Yueh, and S. V. Nghiem

Department of Electrical Engineering and Computer Science
and Research Laboratory of Electronics
Massachusetts Institute of Technology
Cambridge, MA 02139, USA

J. G. Fleischman, S. Ayasli, and R. T. Shin

MIT Lincoln Laboratory
Lexington, MA 02173, USA

Abstract– As an electromagnetic wave propagates through a random scattering medium, such as a forest, its energy is attenuated and random phase fluctuations are induced. The magnitude of the random phase fluctuations induced is important in estimating how well a Synthetic Aperture Radar (SAR) can image objects within the scattering medium. The two-layer random medium model, consisting of a scattering layer between free space and ground, is used to calculate the variance of the phase fluctuations induced between a transmitter located above the random medium and a receiver located below the random medium. The scattering properties of the random medium are characterized by a correlation function of the random permittivity fluctuations. The effective permittivity of the random medium is first calculated using the strong fluctuation theory, which accounts for large permittivity fluctuations of the scatterers. The distorted Born approximation is used to calculate the first-order scattered field. A perturbation series for the phase of the received field in the Rytov approximation is then introduced and the variance of the phase fluctuations is solved to first order in the permittivity fluctuations. The variance of the phase fluctuations is also calculated assuming that the transmitter and receiver are in the paraxial limit of the random medium, which allows an analytic solution to be obtained. Results are compared using the paraxial appromination, scalar Green's function formulation, and dyadic Green's function formulation. The effects studied are the dependence of the variance of the phase fluctuations on receiver location in lossy and lossless regions, medium thickness, correlation length and fractional volume of scatterers, depolarization of the incident wave, ground layer permittivity, angle of incidence, and polarization.

1. INTRODUCTION

As an electromagnetic wave propagates through a random scattering medium, its energy is attenuated and random phase fluctuations are induced. The ability to calculate these phase fluctuations is of practical interest. Members of the remote sensing community interested in using SAR to detect and image objects within scattering media must use this information as an integral part of their system design. A forest is an example of such a scattering medium, where fluctuations in the density and distribution of foliage induces random phase fluctuations. These

phase fluctuations spread the target return into neighboring range–Doppler cells, thus smearing the image. The magnitude of these fluctuations determines the extent of the range–Doppler spreading and hence gives an estimate of how well targets under foliage can be imaged. The objective of this work is to calculate the phase fluctuations that an electromagnetic wave undergoes as it propagates through a random medium.

The random medium model can be analyzed by using the wave theory approach [1]. This approach begins with Maxwell's equations and develops solutions for the electric field after taking into account absorption and scattering by the medium. The wave theory approach has often been used for studying wave propagation and scattering in continuous random media. Tatarskii and Gertsenshtein [2] studied the propagation of a scalar wave in a homogeneous isotropic medium with quasistatic fluctuations. Lee and Kong [3] studied wave propagation and scattering in a two-layer anisotropic random medium using the bilocal and the nonlinear approximations. They calculated the effective propagation constants of the four characteristic waves associated with the coherent vector fields propagating in an anisotropic random medium, which correspond to the upward- and downward-propagating vectors of the ordinary and extraordinary waves.

The wave theory approach has also been used to calculate backscattering cross sections for continuous random media with lateral and vertical correlations. This has been done by Tsang and Kong [4], Zuniga et al. [5,6], Zuniga and Kong [7], Lin et al. [8], and Borgeaud et al. [9–11]. Stogryn [12] used the first-order renormalization method on a spherically symmetric correlation function, and Fung and Fung [13] used the same method on a cylindrically symmetric correlation function. The modeling of vegetation using the random medium model and wave theory has also been applied by de Wolf [14], Rosenbaum and Bowles [15], Tan et al. [16], Chuah and Tan [17], Tsang and Kong [18], and Nghiem et al. [19].

In this paper, the wave theory approach is used to calculate the variance of the phase fluctuations. In Section 2, the problem is formulated and the random medium model introduced. In Section 3, calculations using the paraxial approximation are shown. In Section 4, calculations using the two-layer dyadic Green's function are discussed. In Section 5, numerical results are presented, and in Section 6, a brief summary is given.

2. FORMULATION

Distorted Born Approximation and Strong Fluctuation Theory

The distorted Born approximation and the strong fluctuation theory are used to calculate the transmitted scattered field. The total electric field transmitted through the random medium to the region of the receiver is (see Figs. 1 and 2)

$$\overline{E}_t(\overline{r}) = \overline{E}_t^{(0)}(\overline{r}) + \overline{E}_{ts}(\overline{r}) \tag{1}$$

where the scattered or incoherent electric field, $\overline{E}_{ts}(\overline{r})$, is found by using the distorted Born approximation [20] and is

$$\overline{E}_{ts}(\overline{r}) \simeq k_0^2 \iiint_{V_1} d^3\overline{r}_1 \, \overline{\overline{G}}_{21}(\overline{r},\overline{r}_1) \cdot \xi(\overline{r}_1) \overline{E}_1^{(0)}(\overline{r}_1) \tag{2}$$

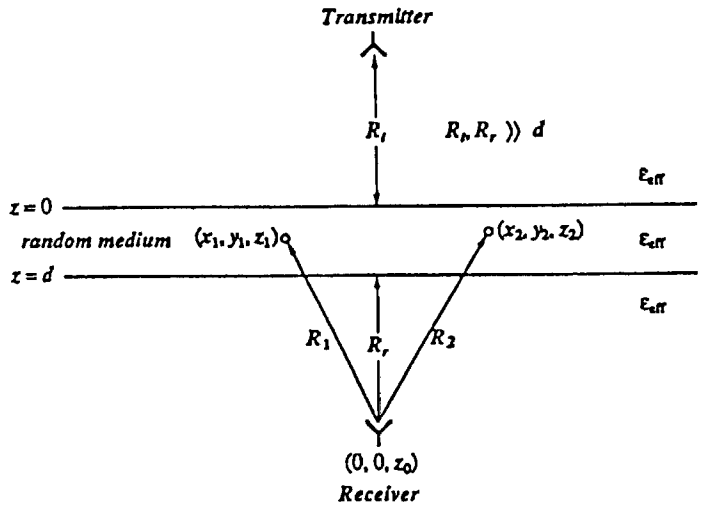

Figure 1. Geometrical configuration for phase fluctuation calculation in the paraxial limit.

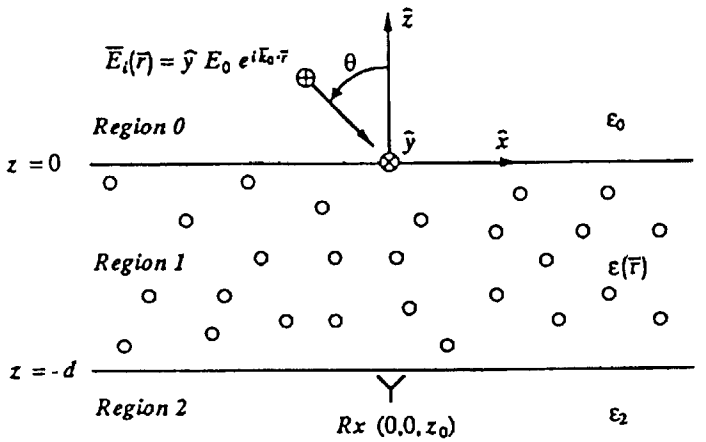

Figure 2. Geometrical configuration for phase fluctuation calculation using two layer dyadic Green's function formulation.

The fields $\overline{E}_1^{(0)}(\overline{r})$ and $\overline{E}_t^{(0)}(\overline{r})$ are the zeroth-order mean or coherent fields in Regions 1 and 2, respectively. The dyadic Green's function, $\overline{\overline{G}}_{21}$, is defined in Appendix A.

The renormalized scattering source, $\xi(\overline{r})$, is obtained using the strong fluctuation theory [20,21]. It is specified as

$$\xi(\overline{r}) = 3\frac{\epsilon_g}{\epsilon_0}\left(\frac{\epsilon(\overline{r})-\epsilon_g}{\epsilon(\overline{r})+2\,\epsilon_g}\right) \tag{3}$$

and ϵ_g is determined by requiring

$$\langle \xi(\overline{r}) \rangle = 0 \tag{4}$$

that is,

$$f\left(\frac{\epsilon_s-\epsilon_g}{\epsilon_s+2\epsilon_g}\right) + (1-f)\left(\frac{\epsilon_0-\epsilon_g}{\epsilon_0+2\epsilon_g}\right) = 0 \tag{5}$$

where f is the fractional volume of the scatterers and ϵ_s is the permittivity of the scatterers.

In the low frequency limit, the effective permittivity is given by [20–24]

$$\epsilon_{eff} = \epsilon_g + \epsilon_0\frac{2}{3}k_0^2\int_0^\infty dr\, r\, C_\xi(\overline{r}) + i\frac{2}{3}k_0^2\,k_g\,\epsilon_0\,U \tag{6}$$

where

$$U = \int_0^\infty dr\, r^2\, C_\xi(\overline{r}) \tag{7}$$

$$C_\xi(\overline{r}) = \delta\, e^{-r/l} \tag{8}$$

C_ξ is a spherically symmetric correlation function of $\xi(\overline{r})$, where δ is the variance of $\xi(\overline{r})$ and l is the correlation length of $\xi(\overline{r})$ and roughly approximates the size of the scatterers.

Scalar Green's Function

When all the depolarization effects and boundary effects are neglected, a scalar Green's function is obtained. This Green's function is used in the paraxial approximation, and is also used to calculate the variance of the phase fluctuations with the receiver at arbitrary distances from the random medium. In this paper, the calculations are shown only for the paraxial approximation.

When depolarization and boundary effects are neglected, the dyadic Green's function in (2) is replaced by a scalar Green's function. Therefore, the scattered field for this approximation is written as

$$\overline{E}_{ts}(\overline{r}) \simeq k_0^2 \iiint_{V_1} d^3\overline{r}_1\, G(\overline{r},\overline{r}_1)\,\xi(\overline{r}_1)\,\overline{E}_t^{(0)}(\overline{r}_1) \tag{9}$$

where the scalar Green's function is [25]

$$G(\overline{r}) = \frac{i}{(2\pi)^2}\iint_{-\infty}^{+\infty} d^2\overline{k}_\perp \frac{1}{2\,k_z}\, e^{i\overline{k}_\perp\cdot\overline{r}_\perp - ik_z z} \tag{10}$$

$$= \frac{e^{ik_{eff}R}}{4\,\pi\,R} \tag{11}$$

and $\overline{k}_\perp = k_x\hat{x} + k_y\hat{y}$, $\overline{r}_\perp = x\hat{x} + y\hat{y}$, $k_z = \sqrt{k_{eff}^2 - k_x^2 - k_y^2}$. R is the distance from a scatterer in the random medium to the receiver (see Fig. 1). Note that this formulation assumes that the permittivity of the regions above and below the random medium are the same as the effective permittivity of the random medium.

Paraxial Approximation

When the distance that the receiver is from the random medium, R_r in Fig. 1, is assumed to be much greater than the thickness of the medium and the correlation length of $\xi(\overline{r})$, then the paraxial approximation can be made. The result of this approximation is that the scalar Green's function can be expressed as

$$G(\overline{r}) = \frac{e^{ik_{eff}R}}{4\,\pi\,R} \simeq \frac{\exp\left\{i\,k_{eff}\left[(z_0-z_1)+\frac{x_1^2+y_1^2}{2(z_0-z_1)}\right]\right\}}{4\,\pi\,(z_0-z_1)} \tag{12}$$

The details of this approximation are discussed in Section 3.

Phase Fluctuations

In calculating the phase fluctuations of the received field, a perturbation series in the phase of the received field is introduced for each polarization. Hence, to find the phase fluctuations for H-Polarization, an incident field polarized in the h-direction is used and the complex phase is calculated for this case. The same is done for an incident field polarized in the v-direction to find the phase fluctuations for V-Polarization.

To find the phase fluctuations for H-Polarization, the total field in Region 2 is written in the Rytov approximation as

$$E_{2h}(\overline{r}) = E_{2h}^{(0)}(\overline{r})\,e^{i\Phi_h(\overline{r})} \simeq E_{2h}^{(0)}(\overline{r}) + E_{2sh}(\overline{r}) \tag{13}$$

where $\Phi_h(\overline{r})$ is the complex phase for H-Polarization, and the subscript h denotes horizontally-polarized fields.

Assuming small fluctuations, it is appropriate to approximate the exponential $e^{i\Phi_h(\overline{r})}$ in (13) by the first two terms of its Taylor series expansion. Note that this assumption is valid for the numerical results illustrated in Section 5, whose standard deviation is in general smaller than 20 degrees. The solution for the complex phases is

$$\Phi_h(\overline{r}) \simeq -i\frac{E_{2sh}(\overline{r})}{E_{2h}^{(0)}(\overline{r})}, \qquad \Phi_v(\overline{r}) \simeq -i\frac{E_{2sv}(\overline{r})}{E_{2v}^{(0)}(\overline{r})} \tag{14}$$

The complex phase, $\Phi(\overline{r})$, contains both phase and amplitude fluctuation information, and can be written explicitly in terms of its real and imaginary parts as $\Phi(\overline{r}) = \psi(\overline{r}) + i\alpha(\overline{r})$, where $\psi(\overline{r})$ and $\alpha(\overline{r})$ correspond to phase and amplitude fluctuations, respectively. To extract the phase fluctuation information, the quantities $\langle\Phi_h(\overline{r}_a)\,\Phi_h^*(\overline{r}_a)\rangle$, $\langle\Phi_h(\overline{r}_a)\,\Phi_h(\overline{r}_a)\rangle$, $\langle\Phi_v(\overline{r}_a)\,\Phi_v^*(\overline{r}_a)\rangle$, and $\langle\Phi_v(\overline{r}_a)\,\Phi_v(\overline{r}_a)\rangle$ must be found. The variances are then

$$\sigma^2_{\psi_h} = \left\langle \psi_h^2 \right\rangle = \frac{\left\langle \Phi_h(\bar{r}_a)\,\Phi_h^*(\bar{r}_a)\right\rangle + \mathrm{Re}\left\langle \Phi_h(\bar{r}_a)\,\Phi_h(\bar{r}_a)\right\rangle}{2} \tag{15}$$

$$\sigma^2_{\psi_v} = \left\langle \psi_v^2 \right\rangle = \frac{\left\langle \Phi_v(\bar{r}_a)\,\Phi_v^*(\bar{r}_a)\right\rangle + \mathrm{Re}\left\langle \Phi_v(\bar{r}_a)\,\Phi_v(\bar{r}_a)\right\rangle}{2} \tag{16}$$

For the scalar Green's function and the paraxial approximation, no distinction is made between the polarizations. Therefore,

$$\Phi(\bar{r}) = \Phi_h(\bar{r}) = \Phi_v(\bar{r}) \simeq -i\,\frac{E_{ts}(\bar{r})}{E_t^{(0)}(\bar{r})} \tag{17}$$

and the variance is calculated as shown above using this value of $\Phi(\bar{r})$.

3. PARAXIAL APPROXIMATION METHOD

The variance of the phase fluctuations for the case of a transmitter and a receiver located far away from the random medium (in the paraxial limit) is calculated in this section. The configuration is shown in Fig. 1. This problem is motivated by the fact that the results are simpler and obtainable in closed form. The closed form results will be used to verify the validity of the numerical results obtained by using the Green's function approach in the following section.

The incident field is assumed to be a plane wave normally incident on the random medium in the z direction (for this formulation the positive z-axis points downward), and is written as

$$\overline{E}_i(\bar{r}) = \hat{x}\, e^{ik_{eff}z} \tag{18}$$

The expression for the complex phase is

$$\Phi(\bar{r}) \simeq -i\, e^{-ik_{eff}z}\, k_0^2 \iiint_{V_1} d^3\bar{r}_1\, \frac{e^{ik_{eff}R_1}}{4\pi R_1}\, \xi(\bar{r}_1)\, e^{ik_{eff}z_1} \tag{19}$$

Calculation of $\langle \Phi(\bar{r}_a)\,\Phi^*(\bar{r}_a)\rangle$

The expression for $\langle \Phi(\bar{r}_a)\,\Phi^*(\bar{r}_a)\rangle$ is obtained from (19) and is

$$\langle \Phi(\bar{r}_a)\,\Phi^*(\bar{r}_a)\rangle = \frac{k_0^4}{(4\pi)^2} \iiint_{V_1} d^3\bar{r}_1 \iiint_{V_2} d^3\bar{r}_2\, \frac{\langle \xi(\bar{r}_1)\xi^*(\bar{r}_2)\rangle}{R_1 R_2} \times e^{ik_{eff}(z_1+R_1-z_0)}\, e^{-ik^*_{eff}\,(z_2+R_2-z_0)} \tag{20}$$

From Fig. 1, R_1 can be written in cartesian coordinates as

$$R_1 = \sqrt{x_1^2 + y_1^2 + (z_0 - z_1)^2} \tag{21}$$

and R_2 can be written in a similar manner. In the paraxial approximation, the scatterers that will contribute to the received scattered field will be limited to those close to the transmitter–receiver axis (close relative to the scatterer-to-receiver distance). This means that the transverse coordinates of the contributing scatterers, $x_{1,2}$ and $y_{1,2}$, will be small relative to the distances to the receiver, $(z_0 - z_{1,2})$. The reason that the contributing scatterers are limited to those close to the transmitter-receiver axis is that the farther off-axis the scatterers are, the more rapidly varying their phases become; therefore, contribution can be considered to come from scatterers near the axis because they have stationary phases. Also, the scatterers far off-axis will not contribute as much as those close to the axis because attenuation in the lossy medium will lessen the contribution of those scatterers with the longer path lengths to the receiver. Because the effective values of $x_{1,2}$ and $y_{1,2}$ are small relative to $(z_0 - z_{1,2})$, the following Taylor series expansions of R_1 and R_2 can be taken:

$$R_{1,2} = (z_0 - z_{1,2}) \left(1 + \frac{x_{1,2}^2 + y_{1,2}^2}{2(z_0 - z_{1,2})^2} + \cdots \right) \tag{22}$$

The first term and the first two terms of the above expression are used in the magnitudes and phases of (20), respectively.

For the receiver to be in the paraxial limit of the random medium, the distance that the receiver is from the bottom of the medium must be much greater than the thickness of the medium. This means that the thickness becomes a negligible quantity relative to the receiver location. Physically, the receiver is so far away from the medium that the medium appears to be just a "screen" of scatterers. Therefore, the quantities $(z_0 - z_1)$ and $(z_0 - z_2)$ of R_1 and R_2 above are approximated by the receiver to medium distance, R_r.

The $\langle \xi(\bar{r}_1)\xi^*(\bar{r}_2)\rangle$ term corresponds to the correlation function introduced in Section 2. It is written in cartesian coordinates as

$$C(\bar{r}_1 - \bar{r}_2) = \delta\, e^{-\sqrt{(x_1-x_2)^2+(y_1-y_2)^2+(z_1-z_2)^2}/l} \tag{23}$$

where δ is the variance and l is the correlation length of $\xi(\bar{r})$. A spherically symmetric correlation function is used for analytic convenience.

The following change of variables is performed to eliminate the dependence of the correlation function on three of the integrations:

$$x_c = \frac{x_1 + x_2}{2},\quad y_c = \frac{y_1 + y_2}{2},\quad z_c = \frac{z_1 + z_2}{2} \tag{24}$$

$$x_d = \frac{x_1 - x_2}{2},\quad y_d = \frac{y_1 - y_2}{2},\quad z_d = \frac{z_1 - z_2}{2} \tag{25}$$

The Jacobian for this coordinate change equals eight. After implementing the change of variables and simplifying terms, the resulting expression is

$$\langle \Phi(\bar{r}_a)\,\Phi^*(\bar{r}_a)\rangle = \frac{\delta\, k_0^4}{2\,\pi^2\, R_r^2} \iiint_{V_c} d^3\bar{r}_c \iiint_{V_d} d^3\bar{r}_d\, \exp\left\{ -\frac{2}{l}\sqrt{x_d^2 + y_d^2 + z_d^2} \right\} \times \exp\left\{ -\frac{k''_{eff}}{R_r}\, x_c^2 \right\} \exp\left\{ i\frac{k'_{eff}}{R_r}\, 2x_d x_c \right\} \exp\left\{ -\frac{k''_{eff}}{R_r}\, y_c^2 \right\} \times \exp\left\{ i\frac{k'_{eff}}{R_r}\, 2y_d y_c \right\} \exp\left\{ -\frac{k''_{eff}}{R_r}(x_d^2 + y_d^2) \right\} \tag{26}$$

where k'_{eff} and k''_{eff} are the real and imaginary parts of k_{eff}, respectively.

After carrying out the integrations over x_c and y_c analytically, the exponentials of order x_d^2 and y_d^2 are neglected. This is valid because in order for the correlation function to be non-zero, x_d and y_d must be smaller than l, which is a small quantity, and it has been assumed that R_r is much greater than l. Assuming that the thickness of the medium, d, is much greater than l and making use of the Laplace method for the integration of z_d, the final expression for $\langle \Phi(\overline{r}_a)\, \Phi^*(\overline{r}_a) \rangle$ is

$$\langle \Phi(\overline{r}_a)\, \Phi^*(\overline{r}_a) \rangle = \frac{\delta\, k_0^4\, d\, l^3}{2\, R_r\, k''_{eff}} \tag{27}$$

Calculation of $\langle \Phi(\overline{r}_a)\, \Phi(\overline{r}_a) \rangle$

The expression for $\langle \Phi(\overline{r}_a)\, \Phi(\overline{r}_a) \rangle$ is obtained from the expression for $\Phi(\overline{r})$ in (19), and has the same form as (20). A $\langle \xi(\overline{r}_1) \xi(\overline{r}_2) \rangle$ term is obtained and is a correlation function similar to the one used in the previous subsection, except the complex variance of $\xi(\overline{r})$, δ_0, is used instead of δ.

The same approximations for R_1, R_2, $z_0 - z_1$, and $z_0 - z_2$ that were made in the previous subsection are made here, and the same change of variables is also made. After these approximations and substitutions are made and the resulting expression simplified, the following is obtained:

$$\langle \Phi(\overline{r}_a)\, \Phi(\overline{r}_a) \rangle = -\frac{\delta_0\, k_0^4}{2\,\pi^2\, R_r^2} \iiint_{V_c} d^3\overline{r}_c \iiint_{V_d} d^3\overline{r}_d \, \exp\left\{ -\frac{2}{l}\sqrt{x_d^2 + y_d^2 + z_d^2} \right\} \times \exp\left\{ i \frac{k_{eff}}{R_r} \left(x_c^2 + x_d^2 + y_c^2 + y_d^2 \right) \right\} \tag{28}$$

The integrations over x_c and y_c are carried out exactly. The exponentials of order x_d^2 and y_d^2 are again neglected. The remaining integrations and the integrand are now the same as in the previous subsection, and are carried out in the same manner. The final result is

$$\langle \Phi(\overline{r}_a)\, \Phi(\overline{r}_a) \rangle = -\frac{\delta_0\, k_0^4\, i\, d\, l^3}{2\, R_r\, k_{eff}} \tag{29}$$

which is similar in form to the result for $\langle \Phi(\overline{r}_a)\, \Phi^*(\overline{r}_a) \rangle$.

4. DYADIC GREEN'S FUNCTION METHOD

The variance of the phase fluctuations for the case of a plane wave incident on a random medium at arbitrary angles of incidence and accounting for boundary and depolarization effects is calculated in this section. The two-layer dyadic Green's function is used in these calculations, and is the most general of the formulations used in this study. The configuration for this problem is shown in Fig. 2. This is the configuration for the general two-layer problem, where there are three distinct regions separated by two boundaries. The permittivity of each of the three regions can be specified, but for this study, Region 0 is assumed to be free space.

Calculations for H-Polarization

The incident and mean fields are (for this formulation the positive z-axis points upward)

$$\overline{E}_i(\overline{r}) = \hat{y}\, e^{i\overline{k}_{m\perp}\cdot\overline{r}_\perp}\, e^{-ik_{0zm}z} = \hat{y}\, e^{ik_{xm}x}\, e^{-ik_{0zm}z} \tag{30}$$

$$\overline{E}_1^{(0)}(\overline{r}) = \hat{y} \left[B_1^{\mathrm{TE}}\, e^{-ik_{1zm}z} + A_1^{\mathrm{TE}}\, e^{ik_{1zm}z} \right] e^{ik_{xm}x} \tag{31}$$

$$\overline{E}_2^{(0)}(\overline{r}) = \hat{y}\, T_m^{\mathrm{TE}}\, e^{-ik_{2zm}z}\, e^{ik_{xm}x} \tag{32}$$

where the z-directed wavenumbers in the expressions above are the mean wavenumbers in each of the regions and it has been assumed that the incident field is polarized in the y-direction and propagating in the x- and z-directions. The up-going and down-going waves in each of the regions consist of an infinite series of waves, the sums of which are denoted by the coefficients shown above. For TE polarization, the coefficients are determined to be [1]

$$R_m^{\mathrm{TE}} = \frac{R_{01}^{\mathrm{TE}} + R_{12}^{\mathrm{TE}}\, e^{i2k_{1zm}d}}{1 + R_{01}^{\mathrm{TE}}\, R_{12}^{\mathrm{TE}}\, e^{i2k_{1zm}d}} \tag{33}$$

$$T_m^{\mathrm{TE}} = \frac{4\, e^{i(k_{1zm} - k_{2zm})d}}{\left(1 + p_{01}^{\mathrm{TE}}\right)\left(1 + p_{12}^{\mathrm{TE}}\right)\left(1 + R_{01}^{\mathrm{TE}}\, R_{12}^{\mathrm{TE}}\, e^{i2k_{1zm}d}\right)} \tag{34}$$

$$A_1^{\mathrm{TE}} = \frac{R_m^{\mathrm{TE}} + 1}{2} + \frac{k_{0zm}}{2k_{1zm}} \left(R_m^{\mathrm{TE}} - 1 \right) \tag{35}$$

$$B_1^{\mathrm{TE}} = \frac{R_m^{\mathrm{TE}} + 1}{2} - \frac{k_{0zm}}{2k_{1zm}} \left(R_m^{\mathrm{TE}} - 1 \right) \tag{36}$$

where the reflection coefficients, $R_{ij}^{\mathrm{TE,TM}}$, are defined in (84)–(85).

Note that scalar electric fields are used in the expressions for the complex phases in (14). To obtain the scalar fields, the vector fields are dot-multiplied with the appropriate unit vector. For H-Polarization, the scalar scattered field is obtained by dot-multiplying the vector scattered field with $\hat{h}(k_{2zm})$, the unit vector in the region of the receiver. Thus, the scalar scattered field in the region of the receiver is

$$E_{2sh}(\overline{r}) \simeq \hat{h}(k_{2zm}) \cdot k_0^2 \iiint_{V_1} d^3\overline{r}_1\, \overline{\overline{G}}_{21}(\overline{r}, \overline{r}_1) \cdot \xi(\overline{r}_1)\, \overline{E}_1^{(0)}(\overline{r}_1) \tag{37}$$

In order to simplify the equations below, the dot-products of the unit vectors are written in shorthand as follows:

$$\hat{h}(k_{2zm}) \cdot \hat{h}\left(-k_{2z}^{(l)}\right) = \frac{k_{lx}}{\sqrt{k_{lx}^2 + k_{ly}^2}} \equiv \mathrm{HH}_{22}(k_{l\perp}) \tag{38}$$

$$\hat{h}(k_{2zm}) \cdot \hat{v}\left(-k_{2z}^{(l)}\right) = \frac{k_{2z}^{(l)}\, k_{ly}}{k_2 \sqrt{k_{lx}^2 + k_{ly}^2}} \equiv \mathrm{HV}_{22}(k_{l\perp}) \tag{39}$$

$$\hat{h}\left(k_{1z}^{(l)}\right) \cdot \hat{h}(k_{1zm}) = \mathrm{HH}_{22}(k_{l\perp}) \tag{40}$$

$$\hat{h}\left(-k_{1z}^{(l)}\right) \cdot \hat{h}(k_{1zm}) = \mathrm{HH}_{22}(k_{l\perp}) \tag{41}$$

$$\hat{v}\left(k_{1z}^{(l)}\right)\cdot\hat{h}(k_{1zm}) = \frac{-k_{1z}^{(l)}\,k_{ly}}{k_{eff}\sqrt{k_{lx}^2+k_{ly}^2}} \equiv \mathrm{VH}_{11}(k_{l\perp}) \tag{42}$$

$$\hat{v}\left(-k_{1z}^{(l)}\right)\cdot\hat{h}(k_{1zm}) = -\mathrm{VH}_{11}(k_{l\perp}) \tag{43}$$

where the mean unit vectors $\hat{h}(k_{0zm})$, $\hat{h}(k_{1zm})$, and $\hat{h}(k_{2zm})$ are equal to $\hat{y}$ and l equals 1 or 2 corresponding to the integration over $\overline{k}_{1\perp}$ or $\overline{k}_{2\perp}$, respectively. The first two quantities above correspond to the dot-products of the unit vector outside the integral in (37) with the outside vectors of $\overline{\overline{G}}_{21}$. The last four quantities are the dot-products of the inside vectors of the Green's function with the mean electric field in Region 1.

After making the above definitions, the complex phase is

$$\begin{aligned}\Phi_h(\overline{r}) = {} & \frac{e^{ik_{2zm}z}\,k_0^2}{T_m^{\mathrm{TE}}\,e^{ik_{xm}x}\,8\pi^2}\iiint_{V_1} d^3\overline{r}_1 \iint d^2\overline{k}_{1\perp}\frac{e^{i\overline{k}_{1\perp}\cdot(\overline{r}_\perp-\overline{r}_{1\perp})}\,e^{-ik_{2z}(z+d)}\,e^{ik_{1z}d}}{k_{1z}} \\ & \times\left\{\frac{T_{12}^{\mathrm{TE}}(k_{1\perp})}{D_2(k_{1\perp})}\,\mathrm{HH}_{22}(k_{1\perp})\,\mathrm{HH}_{22}(k_{1\perp})\left[R_{10}^{\mathrm{TE}}(k_{1\perp})\,e^{-ik_{1z}z_1}+e^{ik_{1z}z_1}\right]\right. \\ & \left.+\frac{k_{eff}}{k_2}\frac{T_{12}^{\mathrm{TM}}(k_{1\perp})}{F_2(k_{1\perp})}\,\mathrm{HV}_{22}(k_{1\perp})\,\mathrm{VH}_{11}(k_{1\perp})\left[R_{10}^{\mathrm{TM}}(k_{1\perp})\,e^{-ik_{1z}z_1}-e^{ik_{1z}z_1}\right]\right\} \\ & \times\xi(\overline{r}_1)\left[B_1^{\mathrm{TE}}\,e^{-ik_{1zm}z_1}+A_1^{\mathrm{TE}}\,e^{ik_{1zm}z_1}\right]e^{ik_{xm}x_1}\end{aligned} \tag{44}$$

With this expression for the complex phase, the quantities $\langle\Phi_h(\overline{r}_a)\,\Phi_h^*(\overline{r}_a)\rangle$ and $\langle\Phi_h(\overline{r}_a)\,\Phi_h(\overline{r}_a)\rangle$ can be calculated as shown below. For the remainder of this section, the field point $\overline{r}_a$ will not be explicitly written out.

Calculation of $\langle\Phi_h\,\Phi_h^*\rangle$

The expression for $\langle\Phi_h\,\Phi_h^*\rangle$ is obtained from (44) and is

$$\begin{aligned}\langle\Phi_h\,\Phi_h^*\rangle = {} & \frac{k_0^4 e^{i(k_{2zm}-k_{2zm}^*)z}}{64\pi^4 T_m^{\mathrm{TE}}T_m^{\mathrm{TE}^*}e^{i(k_{xm}-k_{xm})x}}\iiint_{V_1} d^3\overline{r}_1\iiint_{V_2} d^3\overline{r}_2\iint d^2\overline{k}_{1\perp}\iint d^2\overline{k}_{2\perp} \\ & \times e^{i\overline{k}_{1\perp}\cdot(\overline{r}_\perp-\overline{r}_{1\perp})}e^{-i\overline{k}_{2\perp}\cdot(\overline{r}_\perp-\overline{r}_{2\perp})}\,e^{-ik_{2z}^{(1)}(z+d)}e^{ik_{2z}^{(2)^*}(z+d)}\,e^{i(k_{1z}^{(1)}-k_{1z}^{(2)^*})d} \\ & \times\left[Ae^{-ik_{1z}^{(1)}z_1}+Be^{ik_{1z}^{(1)}z_1}+Ce^{-ik_{1z}^{(1)}z_1}-De^{ik_{1z}^{(1)}z_1}\right]\left[B_1e^{-ik_{1zm}z_1}+A_1e^{ik_{1zm}z_1}\right] \\ & \times\left[Ee^{ik_{1z}^{(2)^*}z_2}+Fe^{-ik_{1z}^{(2)^*}z_2}+Ge^{ik_{1z}^{(2)^*}z_2}-He^{-ik_{1z}^{(2)^*}z_2}\right]\left[B_1^*e^{ik_{1zm}^*z_2}+A_1^*e^{-ik_{1zm}^*z_2}\right] \\ & \times e^{ik_{xm}x_1}e^{-ik_{xm}x_2}\,\frac{\langle\xi(\overline{r}_1)\xi^*(\overline{r}_2)\rangle}{k_{1z}^{(1)}k_{1z}^{(2)^*}}\end{aligned} \tag{45}$$

where the coefficients A through H are defined in Appendix B and the constants A_1 and B_1 are defined in (33)-(36). Also,

$$k_{1z}^{(1)} = \sqrt{k_{eff}^2-k_{1x}^2-k_{1y}^2}\,, \qquad k_{1z}^{(2)} = \sqrt{k_{eff}^2-k_{2x}^2-k_{2y}^2} \tag{46}$$

$$k_{2z}^{(1)} = \sqrt{k_2^2-k_{1x}^2-k_{1y}^2}\,, \qquad k_{2z}^{(2)} = \sqrt{k_2^2-k_{2x}^2-k_{2y}^2} \tag{47}$$

The superscripts of $k_{1z}^{(1)}$ and $k_{2z}^{(1)}$ associate the z-directed wavenumbers with the integration variable $\overline{k}_{1\perp}$. Likewise, the superscripts of $k_{1z}^{(2)}$ and $k_{2z}^{(2)}$ associate the z-directed wavenumbers with the integration variable $\overline{k}_{2\perp}$. In the above expressions, the mean wavenumber in the x direction, k_{xm}, is real because Region 0 is free-space, and the same in all three regions from phase matching conditions.

The correlation function used is the same spherically symmetric correlation function used in the previous section, but the form which is used is the Fourier transform of the spectral intensity function [1] and is given by

$$C(\overline{r}_1-\overline{r}_2) = \delta\iiint d^3\overline{\beta}\,\frac{l^3}{\pi^2(1+\beta^2l^2)^2}\,e^{-i\overline{\beta}_\perp\cdot(\overline{r}_{1\perp}-\overline{r}_{2\perp})-i\beta_z(z_1-z_2)} \tag{48}$$

where δ is the variance and l is the correlation length of $\xi(\overline{r})$.

Integrating over the perpendicular spatial components, $\overline{r}_{1\perp}$ and $\overline{r}_{2\perp}$, the limits of which are from $-\infty$ to $+\infty$, yields delta functions. Integrating over $\overline{k}_{1\perp}$ and $\overline{k}_{2\perp}$, which are in the arguments of the delta functions and also with the limits of integration from $-\infty$ to $+\infty$, results in the following requirements:

$$\overline{k}_{1\perp} = \overline{k}_{2\perp} = \overline{k}_{m\perp} - \overline{\beta}_\perp \tag{49}$$

$$\Longrightarrow k_{1z}^{(1)} = \sqrt{k_{eff}^2-k_{1\perp}^2} = \sqrt{k_{eff}^2-k_{2\perp}^2} = k_{1z}^{(2)} \tag{50}$$

$$\Longrightarrow k_{2z}^{(1)} = \sqrt{k_2^2-k_{1\perp}^2} = \sqrt{k_2^2-k_{2\perp}^2} = k_{2z}^{(2)} \tag{51}$$

From (50) and (51), it is apparent that the superscripts of $k_{1z}^{(1)}$, $k_{1z}^{(2)}$, $k_{2z}^{(1)}$, and $k_{2z}^{(2)}$ no longer need to be used.

The integrations of z_1 and z_2 are performed next, which leaves the final three integrations from negative to positive infinity over the variable $\overline{\beta}$. The β_z integration is performed using contour integration methods.

After carrying out the β_z integration, the integrand depends only on the variable $\overline{\beta}_\perp$. The last two integrations must be done numerically. To simplify the integral, the integration variables are transformed to cylindrical coordinates so that one of the integrations (the β_ϕ integration) is over finite limits and simpler to perform numerically. The following is the final result for the value of $\langle\Phi_h\,\Phi_h^*\rangle$, which requires two numerical integrations:

$$\begin{aligned}\langle\Phi_h\,\Phi_h^*\rangle = {} & \frac{k_0^4\,\delta\,i\,e^{i(k_{2zm}-k_{2zm}^*)z}}{2\,\pi\,l\,T_m^{\mathrm{TE}}\,T_m^{\mathrm{TE}^*}}\int_0^\infty d\beta_\rho\int_0^{2\pi}d\beta_\phi\,\frac{\beta_\rho}{k_{1z}\,k_{1z}^*}\,e^{id(k_{1z}-k_{1z}^*)} \\ & \times e^{-ik_{2z}(z+d)}\,e^{ik_{2z}^*(z+d)}\sum_{(\alpha_1,\alpha_2,\beta_1,\beta_2)}\left\{\square_{(\alpha_1,\alpha_2,\beta_1,\beta_2)}\,F(\kappa_1,\kappa_2)\right\}\end{aligned} \tag{52}$$

where

$$F(\kappa_1,\kappa_2) = \frac{1-e^{id(\kappa_1-\kappa_2)}}{(\gamma-\kappa_2)^2(-\gamma-\kappa_2)^2(\kappa_1-\kappa_2)}$$

$$- \frac{1}{(2\gamma)^2(\gamma+\kappa_1)(\gamma+\kappa_2)}\left[ide^{id(\gamma+\kappa_1)}+\left(1-e^{id(\gamma+\kappa_1)}\right)\left(\frac{1}{\gamma+\kappa_1}+\frac{1}{\gamma+\kappa_2}+\frac{1}{\gamma}\right)\right]$$
$$- \frac{1}{(2\gamma)^2(-\gamma+\kappa_1)(-\gamma+\kappa_2)}\left[ide^{id(\gamma-\kappa_2)}+\left(e^{id(\gamma-\kappa_2)}-e^{id(\kappa_1-\kappa_2)}\right)\right.$$
$$\left.\times\left(\frac{1}{-\gamma+\kappa_1}+\frac{1}{-\gamma+\kappa_2}-\frac{1}{\gamma}\right)\right] \tag{53}$$

$$\kappa_1 = \alpha_1 k_{1z} + \alpha_2 k_{1zm}, \qquad \alpha_1, \alpha_2 = -1, 1 \tag{54}$$

$$\kappa_2 = \beta_1 k^*_{1z} + \beta_2 k^*_{1zm}, \qquad \beta_1, \beta_2 = -1, 1 \tag{55}$$

$$\gamma = i\sqrt{\beta_x^2 + \beta_y^2 + 1/l^2} \tag{56}$$

$$k_{1z} = \sqrt{k_{eff}^2 - (-\beta_x + k_{xm})^2 - (-\beta_y)^2} \tag{57}$$

$$k_{2z} = \sqrt{k_2^2 - (-\beta_x + k_{xm})^2 - (-\beta_y)^2} \tag{58}$$

$$\beta_x = \beta_\rho \cos\beta_\phi \tag{59}$$

$$\beta_y = \beta_\rho \sin\beta_\phi \tag{60}$$

and the $\square$ coefficients are defined in Appendix B. The three main quantities in the function F are the residues of the poles from the integration of β_z.

Calculation of $\langle \Phi_h \Phi_h \rangle$

The calculation of $\langle \Phi_h \Phi_h \rangle$ parallels the calculation of $\langle \Phi_h \Phi_h^* \rangle$ discussed above. First, the expression for $\langle \Phi_h \Phi_h \rangle$ is obtained using (44), and is very similar to (45). The coefficients A through H are defined in Appendix B. The correlation function used is the same as that used in the previous subsection, (48), except the complex variance of $\xi(\overline{r})$, δ_0, is used instead of δ. Next, the integrations of the perpendicular components, $\overline{r}_{1\perp}$, $\overline{r}_{2\perp}$, $\overline{k}_{1\perp}$, and $\overline{k}_{2\perp}$, are performed using the same methods discussed above. The result of these integrations requires that

$$\overline{k}_{1\perp} = \overline{k}_{m\perp} - \overline{\beta}_\perp \qquad \text{and} \qquad \overline{k}_{2\perp} = \overline{k}_{m\perp} + \overline{\beta}_\perp$$

Note that for this case, $\overline{k}_{1\perp}$ is *not* equal to $\overline{k}_{2\perp}$ as in the previous subsection. The wavenumbers $k_{1z}^{(1)}$, $k_{1z}^{(2)}$, $k_{2z}^{(1)}$, and $k_{2z}^{(2)}$ must still be named differently.

The z_1 and z_2 integrations are performed next, which again leaves the threefold integration over the variable $\overline{\beta}$. Again, the β_z integration is carried out using contour integration methods similar to those used to calculate $\langle \Phi_h \Phi_h^* \rangle$. There is a difference for this case, however, because for normal incidence $k_{1z}^{(1)}$ will equal $k_{1z}^{(2)}$, and thus it is possible for κ_1 to equal κ_2, which yields an additional double-order pole. The result is that the value of one of the residues depends on the values of κ_1 and κ_2, as shown below. The final result requires two numerical

integrations and is

$$\langle \Phi_h \Phi_h \rangle = \frac{i\,k_0^4\,\delta_0\,e^{i2k_{2zm}z}}{2\pi\,l\,T_m^{\mathrm{TE}}\,T_m^{\mathrm{TE}}} \int_0^\infty d\beta_\rho \int_0^{2\pi} d\beta_\phi \frac{\beta_\rho}{k_{1z}^{(1)}\,k_{1z}^{(2)}}\, e^{id(k_{1z}^{(1)}+k_{1z}^{(2)})}$$
$$\times\, e^{-ik_{2z}^{(1)}(z+d)}\, e^{-ik_{2z}^{(2)}(z+d)} \sum_{(\alpha_1,\alpha_2,\beta_1,\beta_2)} \left\{ \square_{(\alpha_1,\alpha_2,\beta_1,\beta_2)}\, G(\kappa_1,\kappa_2) \right\} \tag{62}$$

where

$$G(\kappa_1,\kappa_2) = + \left\{ \begin{array}{c} \dfrac{1-e^{id(\kappa_1-\kappa_2)}}{(\gamma-\kappa_2)^2(-\gamma-\kappa_2)^2(\kappa_1-\kappa_2)} \\ \dfrac{-id}{(\gamma-\kappa_1)^2(-\gamma-\kappa_1)^2} \end{array} \right\}$$
$$- \frac{1}{(2\gamma)^2(\gamma+\kappa_1)(\gamma+\kappa_2)}\left[ide^{id(\gamma+\kappa_1)}+\left(1-e^{id(\gamma+\kappa_1)}\right)\left(\frac{1}{\gamma+\kappa_1}+\frac{1}{\gamma+\kappa_2}+\frac{1}{\gamma}\right)\right]$$
$$- \frac{1}{(2\gamma)^2(-\gamma+\kappa_1)(-\gamma+\kappa_2)}\left[ide^{id(\gamma-\kappa_2)}+\left(e^{id(\gamma-\kappa_2)}-e^{id(\kappa_1-\kappa_2)}\right)\right.$$
$$\left.\times\left(\frac{1}{-\gamma+\kappa_1}+\frac{1}{-\gamma+\kappa_2}-\frac{1}{\gamma}\right)\right], \qquad \left\{ \begin{array}{ll} \text{if} & \kappa_1 \neq \kappa_2 \\ \text{if} & \kappa_1 = \kappa_2 \end{array} \right. \tag{63}$$

$$\kappa_1 = \alpha_1 k_{1z}^{(1)} + \alpha_2 k_{1zm}, \qquad \alpha_1, \alpha_2 = -1, 1 \tag{64}$$

$$\kappa_2 = \beta_1 k_{1z}^{(2)} + \beta_2 k_{1zm}, \qquad \beta_1, \beta_2 = -1, 1 \tag{65}$$

$$k_{1z}^{(1)} = \sqrt{k_{eff}^2 - (-\beta_x + k_{xm})^2 - (-\beta_y)^2} \tag{66}$$

$$k_{1z}^{(2)} = \sqrt{k_{eff}^2 - (\beta_x + k_{xm})^2 - (\beta_y)^2} \tag{67}$$

$$k_{2z}^{(1)} = \sqrt{k_2^2 - (-\beta_x + k_{xm})^2 - (-\beta_y)^2} \tag{68}$$

$$k_{2z}^{(2)} = \sqrt{k_2^2 - (\beta_x + k_{xm})^2 - (\beta_y)^2} \tag{69}$$

and γ, β_x, and β_y are defined previously, (56), (59), and (60).

The four main quantities in the function G are the residues of the poles which result when integrating over β_z, where only one of the first two residues is used depending on the values of κ_1 and κ_2 as shown.

Calculations for V-Polarization

The calculation of phase fluctuations for V-Polarization is similar to the derivation for H-Polarization, with most of the differences arising from the definitions of the incident and mean fields and the resulting changes in the dot-products of the unit vectors. To begin with, the incident field is polarized in the $\hat{v}$-direction, and the mean fields can be found by using duality and are

$$\overline{E}_1^{(0)}(\overline{r}) = -\eta_1 \left[\hat{v}(-k_{1zm})\, B_1^{\mathrm{TM}}\, e^{-ik_{1zm}z} + \hat{v}(k_{1zm})\, A_1^{\mathrm{TM}}\, e^{ik_{1zm}z} \right] e^{ik_{xm}x} \tag{70}$$

$$\overline{E}_2^{(0)}(\overline{r}) = -\eta_2\,\hat{v}(-k_{2zm})\,T_m^{\rm TM}\,e^{-ik_{2zm}z}\,e^{ik_{xm}x} \tag{71}$$

where η_1 and η_2 are the characteristic impedances of Regions 1 and 2, respectively, and are defined as $\eta = (\mu/\epsilon)^{1/2}$. The coefficients for the up-going and down-going fields are

$$R_m^{\rm TM} = \frac{R_{01}^{\rm TM} + R_{12}^{\rm TM}\,e^{i2k_{1zm}d}}{1 + R_{01}^{\rm TM}\,R_{12}^{\rm TM}\,e^{i2k_{1zm}d}} \tag{72}$$

$$T_m^{\rm TM} = \frac{4\,e^{i(k_{1zm}-k_{2zm})d}}{(1+p_{01}^{\rm TM})\,(1+p_{12}^{\rm TM})\,(1+R_{01}^{\rm TM}\,R_{12}^{\rm TM}\,e^{i2k_{1zm}d})} \tag{73}$$

$$A_1^{\rm TM} = \frac{R_m^{\rm TM}+1}{2} + \frac{k_{0zm}\epsilon_1}{2k_{1zm}\epsilon_0}\left(R_m^{\rm TM}-1\right) \tag{74}$$

$$B_1^{\rm TM} = \frac{R_m^{\rm TM}+1}{2} - \frac{k_{0zm}\epsilon_1}{2k_{1zm}\epsilon_0}\left(R_m^{\rm TM}-1\right) \tag{75}$$

where again, the reflection coefficients, $R_{ij}^{\rm TE,TM}$, are defined in (84)-(85).

To find the complex phase, $\Phi_v(\overline{r})$ in (14), the appropriate scalar fields must be found. For V-Polarization, the scalar scattered field is found by dot-multiplying the vector scattered field by $\hat{v}(-k_{2zm})$, the unit vector in the region of the receiver. Thus, the scalar scattered field in the region of the receiver is

$$E_{2sv}(\overline{r}) \simeq \hat{v}(-k_{2zm})\cdot k_0^2 \iiint_{V_1} d^3\overline{r}_1\,\overline{\overline{G}}_{21}(\overline{r},\overline{r}_1)\cdot\xi(\overline{r}_1)\,\overline{E}_1^{(0)}(\overline{r}_1) \tag{76}$$

To simplify the equations below, the dot-products of two of the unit vectors are written in shorthand as

$$\hat{v}(-k_{2zm})\cdot\hat{h}(-k_{2z}^{(l)}) = \frac{-k_{2zm}\,k_{ly}}{k_2\sqrt{k_{lx}^2+k_{ly}^2}} \equiv {\rm VH}_{22}(k_{l\perp}) \tag{77}$$

$$\hat{v}(-k_{2zm})\cdot\hat{v}(-k_{2z}^{(l)}) = \frac{k_{2zm}\,k_{2z}^{(l)}\,k_{lx}}{k_2^2\sqrt{k_{lx}^2+k_{ly}^2}} + \frac{k_{xm}\sqrt{k_{lx}^2+k_{ly}^2}}{k_2^2} \equiv {\rm VV}_{22}(k_{l\perp}) \tag{78}$$

where the mean unit vectors $\hat{h}(k_{0zm})$, $\hat{h}(k_{1zm})$, $\hat{h}(k_{2zm})$ are equal to $\hat{y}$ and l equals 1 or 2 corresponding to the integration over $\overline{k}_{1\perp}$ or $\overline{k}_{2\perp}$, respectively. The quantities $\rm VH_{22}$ and $\rm VV_{22}$ correspond to the dot-multiplication of the unit vector outside the integral in (76) with the outer vectors of $\overline{\overline{G}}_{21}$.

After making the above definitions, the complex phase is written as

$$\begin{aligned}\Phi_v(\overline{r}) = {} & \frac{e^{ik_{2zm}z}k_0^2}{\eta_2 T_m^{\rm TM} e^{ik_{xm}x}8\pi^2}\iiint_{V_1} d^3\overline{r}_1 \iint d^2\overline{k}_{1\perp}\frac{e^{i\overline{k}_{1\perp}\cdot(\overline{r}_\perp-\overline{r}_{1\perp})}e^{-ik_{2z}(z+d)}e^{ik_{1z}d}}{k_{1z}} \\ & \times\left\{\frac{T_{12}^{\rm TE}(k_{1\perp})}{D_2(k_{1\perp})}VH_{22}(k_{1\perp})\left[R_{10}^{\rm TE}(k_{1\perp})\hat{h}(k_{1z})e^{-ik_{1z}z_1}+\hat{h}(-k_{1z})e^{ik_{1z}z_1}\right]\right. \\ & \left.+\frac{k_{eff}}{k_2}\frac{T_{12}^{\rm TM}(k_{1\perp})}{F_2(k_{1\perp})}VV_{22}(k_{1\perp})\left[R_{10}^{\rm TM}(k_{1\perp})\hat{v}(k_{1z})e^{-ik_{1z}z_1}+\hat{v}(-k_{1z})e^{ik_{1z}z_1}\right]\right\} \\ & \cdot\left[\hat{v}(-k_{1zm})B_1^{\rm TM}e^{-ik_{1zm}z_1}+\hat{v}(k_{1zm})A_1^{\rm TM}e^{ik_{1zm}z_1}\right]\xi(\overline{r}_1)\eta_1 e^{ik_{xm}x_1}\end{aligned} \tag{79}$$

Calculation of $\langle\Phi_v\,\Phi_v^*\rangle$

The expression for $\langle\Phi_v\,\Phi_v^*\rangle$ is obtained from (79). The same steps used to evaluate $\langle\Phi_h\,\Phi_h^*\rangle$ are used to evaluate $\langle\Phi_v\,\Phi_v^*\rangle$. The only major difference is the definition of the $\square$ coefficients, which is shown in Appendix B. The final result is

$$\begin{aligned}\langle\Phi_v\,\Phi_v^*\rangle = {} & \frac{k_0^4\,\delta\,i\,\eta_1\,\eta_1^*\,e^{i(k_{2zm}-k_{2zm}^*)z}}{2\,\pi\,l\,\eta_2\,\eta_2^*\,T_m^{\rm TM}\,T_m^{\rm TM^*}}\int_0^\infty d\beta_\rho\int_0^{2\pi}d\beta_\phi\frac{\beta_\rho}{k_{1z}\,k_{1z}^*}\,e^{id(k_{1z}-k_{1z}^*)} \\ & \times e^{-ik_{2z}(z+d)}\,e^{ik_{2z}^*(z+d)}\sum_{(\alpha_1,\alpha_2,\beta_1,\beta_2)}\left\{\square_{(\alpha_1,\alpha_2,\beta_1,\beta_2)}\,F(\kappa_1,\kappa_2)\right\}\end{aligned} \tag{80}$$

where the values of κ_1, κ_2, γ, k_{1z}, k_{2z}, β_x, and β_y are defined in (54)-(60), and $F(\kappa_1,\kappa_2)$ is defined in (53). This result requires two numerical integrations.

Calculation of $\langle\Phi_v\,\Phi_v\rangle$

From the expression for Φ_v in (79), the expression for $\langle\Phi_v\,\Phi_v\rangle$ can be obtained. The same steps used to calculate $\langle\Phi_h\,\Phi_h\rangle$ are used to calculate $\langle\Phi_v\,\Phi_v\rangle$, with the appropriate coefficients used, shown in Appendix B. The final result requires two numerical integrations and is

$$\begin{aligned}\langle\Phi_v\,\Phi_v\rangle = {} & \frac{k_0^4\,\delta_0\,i\,\eta_1\,\eta_1\,e^{i2k_{2zm}z}}{2\,\pi\,l\,\eta_2\,\eta_2\,T_m^{\rm TM}\,T_m^{\rm TM}}\int_0^\infty d\beta_\rho\int_0^{2\pi}d\beta_\phi\frac{\beta_\rho}{k_{1z}^{(1)}\,k_{1z}^{(2)}}\,e^{id(k_{1z}^{(1)}+k_{1z}^{(2)})} \\ & \times e^{-ik_{2z}^{(1)}(z+d)}\,e^{-ik_{2z}^{(2)}(z+d)}\sum_{(\alpha_1,\alpha_2,\beta_1,\beta_2)}\left\{\square_{(\alpha_1,\alpha_2,\beta_1,\beta_2)}\,G(\kappa_1,\kappa_2)\right\}\end{aligned} \tag{81}$$

where $G(\kappa_1,\kappa_2)$ is defined in (63).

5. RESULTS AND DISCUSSION

In this section, results obtained using the paraxial approximation, the scalar Green's function (introduced in Section 2 and discussed in detail in [26]), and the Dyadic Green's function formulations are compared, showing good agreement between all three methods in the common regions of validity. The dependence of the variance of the phase fluctuations on the medium parameters are next illustrated and discussed.

The first result, shown in Fig. 3, is a plot of the standard deviation of the phase fluctuations as a function of receiver location, R_r, for all three formulations. The plot shows that the results agree well when the receiver is in the paraxial limit. Note that the standard deviation of the phase fluctuations decreases as the receiver distance increases. This is caused by the lossy region between the receiver and the medium; this region has the same permittivity as the effective permittivity of the random medium, which is lossy. Attenuation due to the lossy receiver region causes the effective volume of the contributing scatterers to be less than the free-space case. The relatively fewer number of scatterers which contribute to the received scattered field causes the decrease in the variance of the phase fluctuations. Also note that when the receiver is moved close to the bottom of

the medium (which violates the paraxial limit assumption), the paraxial result (long dashed line) increases without bound, while the Green's function results have finite values.

Also note that the standard deviation of phase fluctuations for the dyadic formulation (solid line) is slightly less than those for the scalar formulation (short dashed line). This effect is caused by the fact that the dyadic formulation accounts for depolarization of the scattered field, while the scalar formulation does not. Depolarization in this sense means that the scattered field from either an H- or V-Polarized incident field will consist of *both* polarizations, each of which has an amplitude less than the amplitude of the incident field. Because the dyadic case was formulated such that the phase fluctuations are calculated for only like polarizations (i.e., both scattered and mean fields polarized in the same direction), and the scalar case does not make a distinction between the polarizations, the dyadic case should yield smaller phase fluctuation variance than the scalar case, as the results show. The depolarization effect is most prominent when the receiver is close to the random medium, and less prominent when the receiver is moved into the paraxial limit. This can be explained by the fact that when the receiver is far from the random medium in a lossy region, attenuation limits the scatterers that contribute to the received field to those close to the transmitter-receiver axis. The scatterers close to the axis are those above the receiver, and the scattered field from these scatterers will be polarized in the same direction as the incident field. Therefore, in the paraxial limit, there is little depolarization.

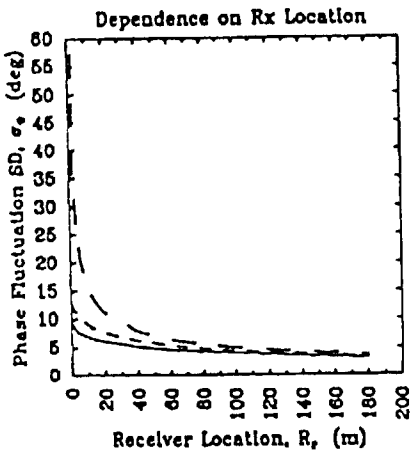

Figure 3. Phase fluctuation standard deviation (SD) dependence on receiver location. Frequency is 1.12 GHz, $\epsilon_s = (39.917 + i\,16.25678)\,\epsilon_0$, $l = 5.2$ mm, $f = 1.67\,\%$, $d = 10.0$ m, and $\epsilon_{eff} = (1.0505 + i\,0.001794)\,\epsilon_0$. Solid line: dyadic formulation; short dashed line: scalar formulation; long dashed line: paraxial approximation.

In Fig. 4, the standard deviation of the phase fluctuations is plotted as a function of receiver location when Region 2 is lossy (solid line), and lossless (dashed line). All the other parameters are the same as in Fig. 3. The purpose of this illustration is to verify the explanation of decreasing phase fluctuation standard deviation as a function of receiver location discussed above. As shown in Fig. 4, the standard deviation of the phase fluctuations does *not* decrease when the receiver is moved away from the random medium in a lossless region (dashed line). This is because when the receiver is moved away from the random medium, more scatterers contribute to the received scattered field since the distance that the scatterers can be from the transmitter-receiver axis before their phases vary too rapidly increases. The transverse region of contributing scatterers should increase in proportion to the medium to receiver distance, R_r, which means that the area of scatterers increases in proportion to R_r^2. However, the power received from each of these scatterers is decreasing by $1/R_r^2$ due to the free-space path loss of the spherical waves from the scatterers. The net result is that when Region 2 is lossless, the received scattered power should change little when R_r is changed. As discussed above, the standard deviation of the phase fluctuations decreases when the receiver is moved away from the random medium in a lossy region because attenuation will decrease the number of scatterers that should contribute to the received scattered field.

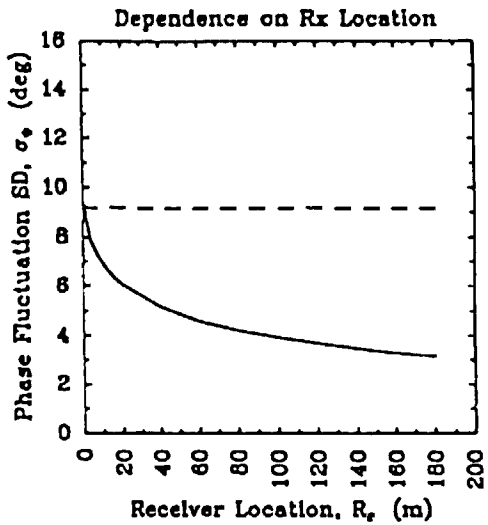

Figure 4. Phase fluctuation standard deviation (SD) for lossy and lossless Region 2. Frequency is 1.12 GHz, $\epsilon_s = (39.917 + i\,16.25678)\epsilon_0$, $l = 5.2$ mm, $f = 1.67\,\%$, $d = 10.0$ m, and $\epsilon_{eff} = (1.0505 + i\,0.001794)\epsilon_0$. Solid line: $\epsilon_2 = (1.0505 + i\,0.001794)\epsilon_0$; dashed line: $\epsilon_2 = (1.0505 + i\,0.0)\epsilon_0$.

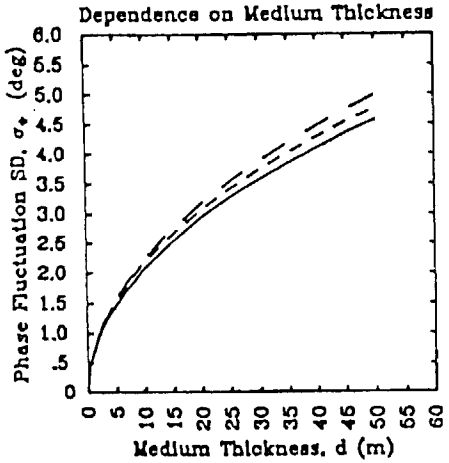

Figure 5. Phase fluctuation standard deviation (SD) dependence on medium thickness. Frequency is 1.12 GHz, $\epsilon_s = (39.917 + i\,16.25678)\epsilon_0$, $l = 5.2$ mm, $f = 1.67\,\%$, $R_r = 500.0$ m, and $\epsilon_{eff} = (1.0505 + i\,0.001794)\epsilon_0$. Solid line: dyadic formulation; short dashed line: scalar formulation; long dashed line: paraxial approximation.

Figure 5 shows the dependence of the phase fluctuation standard deviation on medium thickness, d, for all three formulations. The receiver is located in the paraxial limit and Region 2 has the same permittivity as the effective permittivity of Region 1. The plot shows good agreement between all the results. The behavior of the phase fluctuation standard deviation as a function of medium thickness is governed by two effects. First, increasing the thickness increases the number of scatterers in the medium, which causes an increase in scattering and hence an increase in the phase fluctuation variance. On the other hand, the increased thickness also increases the propagation path of the wave through a lossy medium, thereby reducing the effective number of scatterers which contribute to the received scattered field to those closest to the receiver. As seen in Fig. 5, for small thicknesses, the standard deviation of the phase fluctuations increases relatively rapidly when medium thickness is increased, in accordance with the argument that the increased number of scatterers causes an increase in the phase fluctuation variance. For larger medium thicknesses, the phase fluctuation standard deviation increases relatively slowly as the thickness is increased, and this is in accordance with the argument that the number of effective scatterers is not increasing as rapidly.

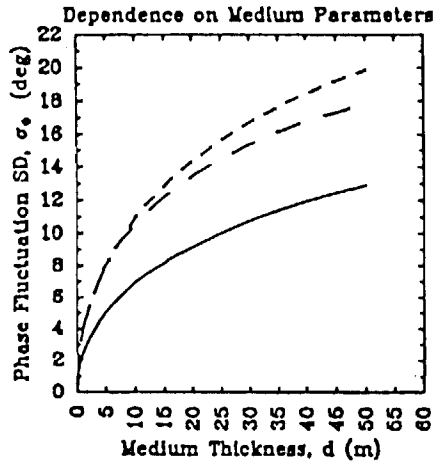

Figure 6. Phase fluctuation standard deviation (SD) dependence on medium parameters. Frequency is 1.12 GHz, $\epsilon_s = (39.917 + i\,16.25678)\epsilon_0$, $R_r = 0.0$ m, and $\epsilon_2 = (6.0 + i\,0.6)\epsilon_0$. Solid line: $l = 5.2$ mm, $f = 1.67\,\%$, $\epsilon_{eff} = (1.0505 + i\,0.001794)\epsilon_0$; short dashed line: $l = 7.2$ mm, $f = 1.67\,\%$, $\epsilon_{eff} = (1.0516 + i\,0.002417)\epsilon_0$; long dashed line: $l = 5.2$ mm, $f = 4.17\,\%$, $\epsilon_{eff} = (1.1360 + i\,0.005478)\epsilon_0$.

In Fig. 6, the dependence of the phase fluctuation standard deviation on the medium parameters of correlation length and fractional volume of scatterers is illustrated. For this case, the permittivity of Region 2 is set to approximately that of the earth at 1.12 GHz, $\epsilon_2 = (6.0 + i\,0.6)\epsilon_0$, and the receiver is directly below the random medium. When the correlation length is increased (solid line versus short dashed line), the phase fluctuation standard deviation also increases, which is due to the fact that the scatterers are larger and thus cause more scattering. When the fractional volume of scatterers is increased (solid line versus long dashed line), the phase fluctuation standard deviation also increases. This is because increasing the fractional volume increases the number of scatterers, and this also causes more scattering to occur.

Figure 7 shows the dependence of the phase fluctuation standard deviation on the permittivity of the ground layer. The results show that for a given medium thickness, the phase fluctuations increase when the ground layer permittivity increases. This is because increasing the ground layer permittivity increases the reflectivity of the lower boundary, which reflects more of the incident energy back into the medium to be scattered. This increased scattering will in turn increase the phase fluctuation of the received field.

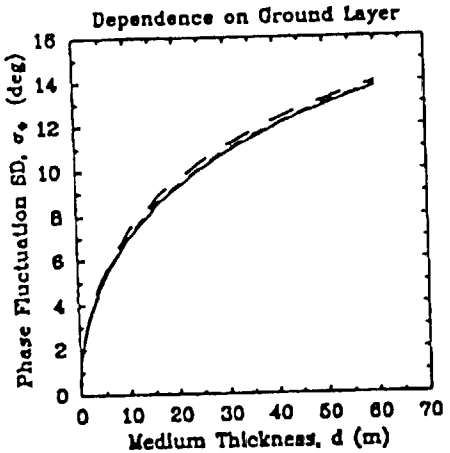

Figure 7. Phase fluctuation standard deviation (SD) dependence on ground layer permittivity. Frequency is 1.12 GHz, $\epsilon_s = (39.917 + i\,16.25678)\epsilon_0$, $l = 5.2$ mm, $f = 1.67\,\%$, $R_r = 0.0$ m, and $\epsilon_{eff} = (1.0505 + i\,0.001794)\epsilon_0$. Solid line: $\epsilon_2 = (6.0 + i\,0.6)\epsilon_0$; short dashed line: $\epsilon_2 = (10.0 + i\,1.0)\epsilon_0$; long dashed line: $\epsilon_2 = (20.0 + i\,3.0)\epsilon_0$.

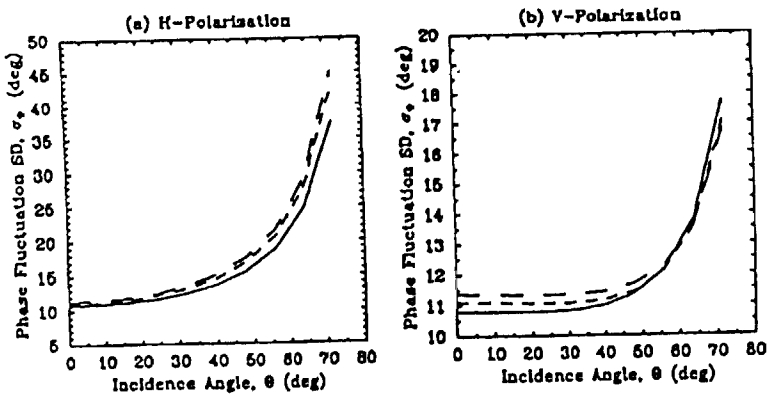

Figure 8. Phase fluctuation standard deviation (SD) dependence on incidence angle. Frequency is 1.12 GHz, $\epsilon_s = (39.917 + i\,16.25678)\epsilon_0$, $l = 5.2$ mm, $f = 1.67\,\%$, $R_r = 0.0$ m, $d = 30.0$ m, and $\epsilon_{eff} = (1.0505 + i\,0.001794)\epsilon_0$. Solid line: $\epsilon_2 = (6.0 + i\,0.6)\epsilon_0$; short dashed line: $\epsilon_2 = (20.0 + i\,3.0)\epsilon_0$; long dashed line: $\epsilon_2 = (40.0 + i\,20.0)\epsilon_0$. (a) H-Polarization. (b) V-Polarization.

Figure 8a shows the phase fluctuation standard deviation dependence on incidence angle for H-Polarization. The figure shows the results for three values of ground layer permittivity. As explained above, when the ground layer permittivity increases for a particular incidence angle, the phase fluctuation standard deviation increases. For all three cases, when the incidence angle increases, the phase fluctuation standard deviation increases. This is partly due to the fact that for greater angles of incidence, the waves propagate through more of the random medium, which increases the amount of scattering. For larger angles of incidence, however, the dominant effect is that for H-Polarization, the reflectivity of the lower boundary is increasing monotonically with increasing incidence angle. As explained previously, if the reflectivity of the lower boundary is increased, more of the incident energy will be reflected back into the medium to be scattered, which increases the phase fluctuations of the received field.

Figure 8b shows the phase fluctuation standard deviation dependence on incidence angle for V-Polarization. The medium parameters and receiver location are the same for this case as for the previous case. Again, the same effect of the ground layer on the phase fluctuation standard deviation is demonstrated in this case as in the previous case, for most angles of incidence. When the incidence angle becomes relatively large, however, the curves cross. Another interesting effect is that the phase fluctuation standard deviation decreases slightly when the incidence angle increases from zero to around 45 degrees. These two effects lead to the conclusion that the reflectivity of the lower boundary, which exhibits a Brewster angle effect for V-Polarization, is again affecting the phase fluctuations. For V-Polarization, when the incidence angle increases, the reflectivity of the lower boundary decreases, drops to a minimum, then increases. This will cause the amount of incident energy reflected back into the random medium to first decrease, go to a minimum, then increase as incidence angle is increased. This explains why the phase fluctuation standard deviation decreases slightly, because less energy is reflected back into the random medium to be scattered. The reason the curves cross can be explained by the fact that the Brewster angle increases for increasing ground layer permittivity. Therefore, the ground layer with the smallest permittivity (solid line) has the smallest Brewster angle, so this curve should reach its minimum and begin increasing before the other curves. Conversely, the ground layer with the largest permittivity (long dashed line) has the largest Brewster angle, so it reaches its minimum and begins to increase after the other curves.

VI. SUMMARY

The variance of the phase fluctuations that an electromagnetic wave undergoes as it propagates through a random medium has been calculated and studied in this paper. This is one of the quantities needed to determine the SAR pattern distortion due to foliage. The other quantity needed is the covariance or autocorrelation of the phase fluctuations, which is calculated in another paper [27]. The effects studied here were the dependence of the variance of the phase fluctuations

on receiver location in lossy and lossless regions, medium thickness, correlation length and fractional volume of scatterers, depolarization of the incident wave, ground layer permittivity, and incidence angle for H- and V-Polarization. The results have been verified by comparing theoretical results obtained using different approaches.

APPENDIX A

The two-layer dyadic Green's function is specified as $\overline{\overline{G}}_{lj}(\overline{r},\overline{r}_1)$, where the subscript l denotes the region of the observation point $\overline{r}$ and the subscript j denotes the region of the source point $\overline{r}_1$. For this study, the observation region (region where the receiver is located) is Region 2, and the source region (region of the scatterers) is Region 1. Therefore, the appropriate Green's function is $\overline{\overline{G}}_{21}$, and is given by (from [1])

$$\overline{\overline{G}}_{21}(\overline{r},\overline{r}_1) = \frac{i}{8\pi^2}\iint_{-\infty}^{+\infty} d^2\overline{k}_{1\perp}\frac{e^{i\overline{k}_{1\perp}\cdot(\overline{r}_\perp-\overline{r}_{1\perp})}e^{-ik_{2z}(z+d)}e^{ik_{1z}d}}{k_{1z}}$$
$$\times\left\{\frac{T_{12}^{\mathrm{TE}}(k_{1\perp})}{D_2(k_{1\perp})}\hat{h}(-k_{2z})\left[R_{10}^{\mathrm{TE}}(k_{1\perp})\hat{h}(k_{1z})e^{-ik_{1z}z_1}+\hat{h}(-k_{1z})e^{ik_{1z}z_1}\right]\right.$$
$$\left.+\frac{k_{eff}}{k_2}\frac{T_{12}^{\mathrm{TM}}(k_{1\perp})}{F_2(k_{1\perp})}\hat{v}(-k_{2z})\left[R_{10}^{\mathrm{TM}}(k_{1\perp})\hat{v}(k_{1z})e^{-ik_{1z}z_1}+\hat{v}(-k_{1z})e^{ik_{1z}z_1}\right]\right\} \quad (82)$$

where

$$D_2(k_{1\perp}) = 1 + R_{01}^{\mathrm{TE}}R_{12}^{\mathrm{TE}}e^{i2k_{1z}d}, \quad F_2(k_{1\perp}) = 1 + R_{01}^{\mathrm{TM}}R_{12}^{\mathrm{TM}}e^{i2k_{1z}d} \quad (83)$$

$$R_{l(l+1)}^{\mathrm{TE}} = \frac{1-p_{l(l+1)}^{\mathrm{TE}}}{1+p_{l(l+1)}^{\mathrm{TE}}}, \quad R_{l(l+1)}^{\mathrm{TM}} = \frac{1-p_{l(l+1)}^{\mathrm{TM}}}{1+p_{l(l+1)}^{\mathrm{TM}}} \quad (84)$$

$$p_{l(l+1)}^{\mathrm{TE}} = \frac{\mu_l k_{(l+1)z}}{\mu_{(l+1)}k_{lz}}, \quad p_{l(l+1)}^{\mathrm{TM}} = \frac{\epsilon_l k_{(l+1)z}}{\epsilon_{(l+1)}k_{lz}} \quad (85)$$

$$T_{l(l+1)}^{\mathrm{TE,TM}} = R_{l(l+1)}^{\mathrm{TE,TM}} + 1 \quad (86)$$

$$k_{1z} = \sqrt{k_{eff}^2 - k_{1x}^2 - k_{1y}^2}, \quad k_{2z} = \sqrt{k_2^2 - k_{1x}^2 - k_{1y}^2} \quad (87)$$

The effective permittivity of the random medium is denoted by k_{eff}. The subscripts of k_{1z} and k_{2z} associate the z-directed wavenumbers with Regions 1 and 2, respectively (see Fig. 2).

The unit vectors $\hat{h}$ and $\hat{v}$ correspond to Transverse Electric polarization (TE, which is horizonal polarization) or Transverse Magnetic polarization (TM, which is vertical polarization), respectively. The unit vector $\hat{h}$ is defined to be

$$\hat{h}(k_{jz}) = \frac{\hat{z}\times\overline{k}_j}{|\hat{z}\times\overline{k}_j|} = \frac{k_x\hat{y}-k_y\hat{x}}{\sqrt{k_x^2+k_y^2}} \quad (88)$$

and the unit vector $\hat{v}$ is defined to be

$$\hat{v}(k_{jz}) = \frac{\overline{k}_j\times\hat{h}(k_{jz})}{k_j} = \frac{-k_{jz}(\hat{x}k_x+\hat{y}k_y)}{k_j\sqrt{k_x^2+k_y^2}} + \hat{z}\frac{\sqrt{k_x^2+k_y^2}}{k_j} \quad (89)$$

where k_{jz} corresponds to the z-directed wavenumber in Region j. Note that (h,v,k) forms a right-handed coordinate system.

APPENDIX B

$\langle\Phi_h(\overline{r}_a)\,\Phi_h^*(\overline{r}_a)\rangle$

The coefficients A through H for $\langle\Phi_h(\overline{r}_a)\,\Phi_h^*(\overline{r}_a)\rangle$ are

$$A = \frac{T_{12}^{\mathrm{TE}}(k_{1\perp})}{D_2(k_{1\perp})}\mathrm{HH}_{22}^2(k_{1\perp})\,R_{10}^{\mathrm{TE}}(k_{1\perp}) \quad (90)$$

$$B = \frac{T_{12}^{\mathrm{TE}}(k_{1\perp})}{D_2(k_{1\perp})}\mathrm{HH}_{22}^2(k_{1\perp}) \quad (91)$$

$$C = \frac{k_{eff}}{k_2}\frac{T_{12}^{\mathrm{TM}}(k_{1\perp})}{F_2(k_{1\perp})}\mathrm{HV}_{22}(k_{1\perp})\,\mathrm{VH}_{11}(k_{1\perp})\,R_{10}^{\mathrm{TM}}(k_{1\perp}) \quad (92)$$

$$D = \frac{k_{eff}}{k_2}\frac{T_{12}^{\mathrm{TM}}(k_{1\perp})}{F_2(k_{1\perp})}\mathrm{HV}_{22}(k_{1\perp})\,\mathrm{VH}_{11}(k_{1\perp}) \quad (93)$$

$$E = \frac{T_{12}^{\mathrm{TE}^*}(k_{2\perp})}{D_2^*(k_{2\perp})}\left(\mathrm{HH}_{22}^*(k_{2\perp})\right)^2\,R_{10}^{\mathrm{TE}^*}(k_{2\perp}) \quad (94)$$

$$F = \frac{T_{12}^{\mathrm{TE}^*}(k_{2\perp})}{D_2^*(k_{2\perp})}\left(\mathrm{HH}_{22}^*(k_{2\perp})\right)^2 \quad (95)$$

$$G = \frac{k_{eff}^*}{k_2^*}\frac{T_{12}^{\mathrm{TM}^*}(k_{2\perp})}{F_2^*(k_{2\perp})}\mathrm{HV}_{22}^*(k_{2\perp})\,\mathrm{VH}_{11}^*(k_{2\perp})\,R_{10}^{\mathrm{TM}^*}(k_{2\perp}) \quad (96)$$

$$H = \frac{k_{eff}^*}{k_2^*}\frac{T_{12}^{\mathrm{TM}^*}(k_{2\perp})}{F_2^*(k_{2\perp})}\mathrm{HV}_{22}^*(k_{2\perp})\,\mathrm{VH}_{11}^*(k_{2\perp}) \quad (97)$$

The $\square$ coefficients for $\langle\Phi_h(\overline{r}_a)\,\Phi_h^*(\overline{r}_a)\rangle$ are

$$\square_{(-1,-1,-1,-1)} = (BF - BH - DF + DH)\,A_1A_1^* \quad (98)$$

$$\square_{(-1,-1,-1,+1)} = (BF - BH - DF + DH)\,A_1B_1^* \quad (99)$$

$$\square_{(-1,-1,+1,-1)} = (BE + BG - DE - DG)\,A_1A_1^* \quad (100)$$

$$\square_{(-1,-1,+1,+1)} = (BE + BG - DE - DG)\,A_1B_1^* \quad (101)$$

$$\square_{(-1,+1,-1,-1)} = (BF - BH - DF + DH)\,B_1A_1^* \quad (102)$$

$$\square_{(-1,+1,-1,+1)} = (BF - BH - DF + DH)\,B_1B_1^* \quad (103)$$

$$\square_{(-1,+1,+1,-1)} = (BE + BG - DE - DG)\,B_1A_1^* \quad (104)$$

$$\square_{(-1,+1,+1,+1)} = (BE + BG - DE - DG)\,B_1B_1^* \quad (105)$$

$$\square_{(+1,-1,-1,-1)} = (AF - AH + CF - CH)\,A_1 A_1^* \tag{106}$$
$$\square_{(+1,-1,-1,+1)} = (AF - AH + CF - CH)\,A_1 B_1^* \tag{107}$$
$$\square_{(+1,-1,+1,-1)} = (AE + AG + CE + CG)\,A_1 A_1^* \tag{108}$$
$$\square_{(+1,-1,+1,+1)} = (AE + AG + CE + CG)\,A_1 B_1^* \tag{109}$$
$$\square_{(+1,+1,-1,-1)} = (AF - AH + CF - CH)\,B_1 A_1^* \tag{110}$$
$$\square_{(+1,+1,-1,+1)} = (AF - AH + CF - CH)\,B_1 B_1^* \tag{111}$$
$$\square_{(+1,+1,+1,-1)} = (AE + AG + CE + CG)\,B_1 A_1^* \tag{112}$$
$$\square_{(+1,+1,+1,+1)} = (AE + AG + CE + CG)\,B_1 B_1^* \tag{113}$$

$\langle \Phi_h(\overline{r}_a)\,\Phi_h(\overline{r}_a)\rangle$

For $\langle \Phi_h(\overline{r}_a)\,\Phi_h(\overline{r}_a)\rangle$, the coefficients A through D are the same as those for $\langle \Phi_h(\overline{r}_a)\,\Phi_h^*(\overline{r}_a)\rangle$ (90)–(93), and the coefficients E through H are the complex conjugates of those in (94)–(97).

The $\square$ coefficients for $\langle \Phi_h(\overline{r}_a)\,\Phi_h(\overline{r}_a)\rangle$ are

$$\square_{(-1,-1,-1,-1)} = (BE + BG - DE - DG)\,A_1 B_1 \tag{114}$$
$$\square_{(-1,-1,-1,+1)} = (BE + BG - DE - DG)\,A_1 A_1 \tag{115}$$
$$\square_{(-1,-1,+1,-1)} = (BF - BH - DF + DH)\,A_1 B_1 \tag{116}$$
$$\square_{(-1,-1,+1,+1)} = (BF - BH - DF + DH)\,A_1 A_1 \tag{117}$$
$$\square_{(-1,+1,-1,-1)} = (BE + BG - DE - DG)\,B_1 B_1 \tag{118}$$
$$\square_{(-1,+1,-1,+1)} = (BE + BG - DE - DG)\,B_1 A_1 \tag{119}$$
$$\square_{(-1,+1,+1,-1)} = (BF - BH - DF + DH)\,B_1 B_1 \tag{120}$$
$$\square_{(-1,+1,+1,+1)} = (BF - BH - DF + DH)\,B_1 A_1 \tag{121}$$
$$\square_{(+1,-1,-1,-1)} = (AE + AG + CE + CG)\,A_1 B_1 \tag{122}$$
$$\square_{(+1,-1,-1,+1)} = (AE + AG + CE + CG)\,A_1 A_1 \tag{123}$$
$$\square_{(+1,-1,+1,-1)} = (AF - AH + CF - CH)\,A_1 B_1 \tag{124}$$
$$\square_{(+1,-1,+1,+1)} = (AF - AH + CF - CH)\,A_1 A_1 \tag{125}$$
$$\square_{(+1,+1,-1,-1)} = (AE + AG + CE + CG)\,B_1 B_1 \tag{126}$$
$$\square_{(+1,+1,-1,+1)} = (AE + AG + CE + CG)\,B_1 A_1 \tag{127}$$
$$\square_{(+1,+1,+1,-1)} = (AF - AH + CF - CH)\,B_1 B_1 \tag{128}$$
$$\square_{(+1,+1,+1,+1)} = (AF - AH + CF - CH)\,B_1 A_1 \tag{129}$$

$\langle \Phi_v(\overline{r}_a)\,\Phi_v^*(\overline{r}_a)\rangle$

The $\square$ coefficients for $\langle \Phi_v(\overline{r}_a)\,\Phi_v^*(\overline{r}_a)\rangle$ are

$$\square_{(-1,-1,-1,-1)} = \left(\overline{B}\cdot\overline{A}_1 + \overline{D}\cdot\overline{A}_1\right)\left(\overline{F}\cdot\overline{A}_1^* + \overline{H}\cdot\overline{A}_1^*\right) \tag{130}$$

$$\square_{(-1,-1,-1,+1)} = \left(\overline{B}\cdot\overline{A}_1 + \overline{D}\cdot\overline{A}_1\right)\left(\overline{F}\cdot\overline{B}_1^* + \overline{H}\cdot\overline{B}_1^*\right) \tag{131}$$
$$\square_{(-1,-1,+1,-1)} = \left(\overline{B}\cdot\overline{A}_1 + \overline{D}\cdot\overline{A}_1\right)\left(\overline{E}\cdot\overline{A}_1^* + \overline{G}\cdot\overline{A}_1^*\right) \tag{132}$$
$$\square_{(-1,-1,+1,+1)} = \left(\overline{B}\cdot\overline{A}_1 + \overline{D}\cdot\overline{A}_1\right)\left(\overline{E}\cdot\overline{B}_1^* + \overline{G}\cdot\overline{B}_1^*\right) \tag{133}$$
$$\square_{(-1,+1,-1,-1)} = \left(\overline{B}\cdot\overline{B}_1 + \overline{D}\cdot\overline{B}_1\right)\left(\overline{F}\cdot\overline{A}_1^* + \overline{H}\cdot\overline{A}_1^*\right) \tag{134}$$
$$\square_{(-1,+1,-1,+1)} = \left(\overline{B}\cdot\overline{B}_1 + \overline{D}\cdot\overline{B}_1\right)\left(\overline{F}\cdot\overline{B}_1^* + \overline{H}\cdot\overline{B}_1^*\right) \tag{135}$$
$$\square_{(-1,+1,+1,-1)} = \left(\overline{B}\cdot\overline{B}_1 + \overline{D}\cdot\overline{B}_1\right)\left(\overline{E}\cdot\overline{A}_1^* + \overline{G}\cdot\overline{A}_1^*\right) \tag{136}$$
$$\square_{(-1,+1,+1,+1)} = \left(\overline{B}\cdot\overline{B}_1 + \overline{D}\cdot\overline{B}_1\right)\left(\overline{E}\cdot\overline{B}_1^* + \overline{G}\cdot\overline{B}_1^*\right) \tag{137}$$
$$\square_{(+1,-1,-1,-1)} = \left(\overline{A}\cdot\overline{A}_1 + \overline{C}\cdot\overline{A}_1\right)\left(\overline{F}\cdot\overline{A}_1^* + \overline{H}\cdot\overline{A}_1^*\right) \tag{138}$$
$$\square_{(+1,-1,-1,+1)} = \left(\overline{A}\cdot\overline{A}_1 + \overline{C}\cdot\overline{A}_1\right)\left(\overline{F}\cdot\overline{B}_1^* + \overline{H}\cdot\overline{B}_1^*\right) \tag{139}$$
$$\square_{(+1,-1,+1,-1)} = \left(\overline{A}\cdot\overline{A}_1 + \overline{C}\cdot\overline{A}_1\right)\left(\overline{E}\cdot\overline{A}_1^* + \overline{G}\cdot\overline{A}_1^*\right) \tag{140}$$
$$\square_{(+1,-1,+1,+1)} = \left(\overline{A}\cdot\overline{A}_1 + \overline{C}\cdot\overline{A}_1\right)\left(\overline{E}\cdot\overline{B}_1^* + \overline{G}\cdot\overline{B}_1^*\right) \tag{141}$$
$$\square_{(+1,+1,-1,-1)} = \left(\overline{A}\cdot\overline{B}_1 + \overline{C}\cdot\overline{B}_1\right)\left(\overline{F}\cdot\overline{A}_1^* + \overline{H}\cdot\overline{A}_1^*\right) \tag{142}$$
$$\square_{(+1,+1,-1,+1)} = \left(\overline{A}\cdot\overline{B}_1 + \overline{C}\cdot\overline{B}_1\right)\left(\overline{F}\cdot\overline{B}_1^* + \overline{H}\cdot\overline{B}_1^*\right) \tag{143}$$
$$\square_{(+1,+1,+1,-1)} = \left(\overline{A}\cdot\overline{B}_1 + \overline{C}\cdot\overline{B}_1\right)\left(\overline{E}\cdot\overline{A}_1^* + \overline{G}\cdot\overline{A}_1^*\right) \tag{144}$$
$$\square_{(+1,+1,+1,+1)} = \left(\overline{A}\cdot\overline{B}_1 + \overline{C}\cdot\overline{B}_1\right)\left(\overline{E}\cdot\overline{B}_1^* + \overline{G}\cdot\overline{B}_1^*\right) \tag{145}$$

where

$$\overline{A} = \frac{T_{12}^{\mathrm{TE}}(k_{1\perp})}{D_2(k_{1\perp})}\,\mathrm{VH}_{22}(k_{1\perp})\,R_{10}^{\mathrm{TE}}(k_{1\perp})\,\hat{h}(k_{1z}^{(1)}) \tag{146}$$
$$\overline{B} = \frac{T_{12}^{\mathrm{TE}}(k_{1\perp})}{D_2(k_{1\perp})}\,\mathrm{VH}_{22}(k_{1\perp})\,\hat{h}(-k_{1z}^{(1)}) \tag{147}$$
$$\overline{C} = \frac{k_{eff}}{k_2}\frac{T_{12}^{\mathrm{TM}}(k_{1\perp})}{F_2(k_{1\perp})}\,\mathrm{VV}_{22}(k_{1\perp})\,R_{10}^{\mathrm{TM}}(k_{1\perp})\,\hat{v}(k_{1z}^{(1)}) \tag{148}$$
$$\overline{D} = \frac{k_{eff}}{k_2}\frac{T_{12}^{\mathrm{TM}}(k_{1\perp})}{F_2(k_{1\perp})}\,\mathrm{VV}_{22}(k_{1\perp})\,\hat{v}(-k_{1z}^{(1)}) \tag{149}$$
$$\overline{E} = \frac{T_{12}^{\mathrm{TE}^*}(k_{2\perp})}{D_2^*(k_{2\perp})}\,\mathrm{VH}_{22}^*(k_{2\perp})\,R_{10}^{\mathrm{TE}^*}(k_{2\perp})\,\hat{h}^*(k_{1z}^{(2)}) \tag{150}$$
$$\overline{F} = \frac{T_{12}^{\mathrm{TE}^*}(k_{2\perp})}{D_2^*(k_{2\perp})}\,\mathrm{VH}_{22}^*(k_{2\perp})\,\hat{h}^*(-k_{1z}^{(2)}) \tag{151}$$
$$\overline{G} = \frac{k_{eff}^*}{k_2^*}\frac{T_{12}^{\mathrm{TM}^*}(k_{2\perp})}{F_2^*(k_{2\perp})}\,\mathrm{VV}_{22}^*(k_{2\perp})\,R_{10}^{\mathrm{TM}^*}(k_{2\perp})\,\hat{v}^*(k_{1z}^{(2)}) \tag{152}$$

$$\overline{H} = \frac{k_{eff}^*}{k_2^*} \frac{T_{12}^{TM^*}(k_{2\perp})}{F_2^*(k_{2\perp})} VV_{22}^*(k_{2\perp})\, \hat{v}^*(-k_{1z}^{(2)}) \tag{153}$$

$$\overline{B}_1 = B_1^{TM}\, \hat{v}(-k_{1zm}) \tag{154}$$

$$\overline{A}_1 = A_1^{TM}\, \hat{v}(k_{1zm}) \tag{155}$$

$\langle \Phi_v(\overline{r}_a)\, \Phi_v(\overline{r}_a) \rangle$

The $\square$ coefficients for $\langle \Phi_v(\overline{r}_a)\, \Phi_v(\overline{r}_a) \rangle$ are

$$\square_{(-1,-1,-1,-1)} = (\overline{B}\cdot\overline{A}_1 + \overline{D}\cdot\overline{A}_1)\ (\overline{E}\cdot\overline{B}_1 + \overline{G}\cdot\overline{B}_1) \tag{156}$$

$$\square_{(-1,-1,-1,+1)} = (\overline{B}\cdot\overline{A}_1 + \overline{D}\cdot\overline{A}_1)\ (\overline{E}\cdot\overline{A}_1 + \overline{G}\cdot\overline{A}_1) \tag{157}$$

$$\square_{(-1,-1,+1,-1)} = (\overline{B}\cdot\overline{A}_1 + \overline{D}\cdot\overline{A}_1)\ (\overline{F}\cdot\overline{B}_1 + \overline{H}\cdot\overline{B}_1) \tag{158}$$

$$\square_{(-1,-1,+1,+1)} = (\overline{B}\cdot\overline{A}_1 + \overline{D}\cdot\overline{A}_1)\ (\overline{F}\cdot\overline{A}_1 + \overline{H}\cdot\overline{A}_1) \tag{159}$$

$$\square_{(-1,+1,-1,-1)} = (\overline{B}\cdot\overline{B}_1 + \overline{D}\cdot\overline{B}_1)\ (\overline{E}\cdot\overline{B}_1 + \overline{G}\cdot\overline{B}_1) \tag{160}$$

$$\square_{(-1,+1,-1,+1)} = (\overline{B}\cdot\overline{B}_1 + \overline{D}\cdot\overline{B}_1)\ (\overline{E}\cdot\overline{A}_1 + \overline{G}\cdot\overline{A}_1) \tag{161}$$

$$\square_{(-1,+1,+1,-1)} = (\overline{B}\cdot\overline{B}_1 + \overline{D}\cdot\overline{B}_1)\ (\overline{F}\cdot\overline{B}_1 + \overline{H}\cdot\overline{B}_1) \tag{162}$$

$$\square_{(-1,+1,+1,+1)} = (\overline{B}\cdot\overline{B}_1 + \overline{D}\cdot\overline{B}_1)\ (\overline{F}\cdot\overline{A}_1 + \overline{H}\cdot\overline{A}_1) \tag{163}$$

$$\square_{(+1,-1,-1,-1)} = (\overline{A}\cdot\overline{A}_1 + \overline{C}\cdot\overline{A}_1)\ (\overline{E}\cdot\overline{B}_1 + \overline{G}\cdot\overline{B}_1) \tag{164}$$

$$\square_{(+1,-1,-1,+1)} = (\overline{A}\cdot\overline{A}_1 + \overline{C}\cdot\overline{A}_1)\ (\overline{E}\cdot\overline{A}_1 + \overline{G}\cdot\overline{A}_1) \tag{165}$$

$$\square_{(+1,-1,+1,-1)} = (\overline{A}\cdot\overline{A}_1 + \overline{C}\cdot\overline{A}_1)\ (\overline{F}\cdot\overline{B}_1 + \overline{H}\cdot\overline{B}_1) \tag{166}$$

$$\square_{(+1,-1,+1,+1)} = (\overline{A}\cdot\overline{A}_1 + \overline{C}\cdot\overline{A}_1)\ (\overline{F}\cdot\overline{A}_1 + \overline{H}\cdot\overline{A}_1) \tag{167}$$

$$\square_{(+1,+1,-1,-1)} = (\overline{A}\cdot\overline{B}_1 + \overline{C}\cdot\overline{B}_1)\ (\overline{E}\cdot\overline{B}_1 + \overline{G}\cdot\overline{B}_1) \tag{168}$$

$$\square_{(+1,+1,-1,+1)} = (\overline{A}\cdot\overline{B}_1 + \overline{C}\cdot\overline{B}_1)\ (\overline{E}\cdot\overline{A}_1 + \overline{G}\cdot\overline{A}_1) \tag{169}$$

$$\square_{(+1,+1,+1,-1)} = (\overline{A}\cdot\overline{B}_1 + \overline{C}\cdot\overline{B}_1)\ (\overline{F}\cdot\overline{B}_1 + \overline{H}\cdot\overline{B}_1) \tag{170}$$

$$\square_{(+1,+1,+1,+1)} = (\overline{A}\cdot\overline{B}_1 + \overline{C}\cdot\overline{B}_1)\ (\overline{F}\cdot\overline{A}_1 + \overline{H}\cdot\overline{A}_1) \tag{171}$$

The coefficients A through D used above are defined in (146)–(149), and the coefficients E through H used above are the complex conjugates of those in (150)–(153).

ACKNOWLEDGEMENTS

This work was supported by the DARPA Contract MDA972-90-C-0021, the ARO Contract DAAL03-88-J-0057, the NASA Contract 958461, the NASA Contract NAGW-1617, and the ONR Contract N00014-89-J-1107.

This work was also sponsored by the Defense Advanced Research Projects Agency. The views expressed are those of the authors and do not reflect the official policy or position of the U. S. Government.

ACKNOWLEDGMENTS

The Editor thanks A. K. Fung and three anonymous Reviewers for reviewing the paper.

REFERENCES

1. Tsang, L., J. A. Kong, and R. T. Shin, *Theory of Microwave Remote Sensing*, Wiley-Interscience, New York, 1985.
2. Tatarskii, V. I., and M. E. Gertsenshtein, "Propagation of waves in a medium with strong fluctuation of the refractive index," *Soviet Physics JETP*, Vol. 17, 458–463, 1963.
3. Lee, J., and J. A. Kong, "Electromagnetic wave scattering in a two-layer anisotropic random medium," *J. Opt. Soc. Am. A*, Vol. 2, 2171–2186, 1985.
4. Tsang, L., and J. A. Kong, "Emissivity of half-space random media," *Radio Science*, Vol. 11, 593–598, 1976.
5. Zuniga, M., T. Habashy, and J. A. Kong, "Active remote sensing of layered random media," *IEEE Transactions on Geoscience Electronics*, Vol. 17, 296–302, 1979.
6. Zuniga, M. A., J. A. Kong, and L. Tsang, "Depolarization effects in the active remote sensing of random media," *J. Appl. Phys.*, Vol. 51, No. 5, 2315–2325, May 1980.
7. Zuniga, M., and J. A. Kong, "Active remote sensing of random media," *J. Appl. Phys.*, Vol. 51, 74–79, 1980.
8. Lin, F. C., J. A. Kong, and R. T. Shin, "Theoretical models for active and passive microwave remote sensing of snow-covered sea ice," *IGARSS'87*, University of Michigan, Ann Arbor, Michigan, 18–21 May 1987.
9. Borgeaud, M., J. A. Kong, and F. C. Lin, "Microwave remote sensing of snow-covered sea ice," *Proceeding of the IGARSS'86 Symposium*, 133–138, Zürich, 8–11 Sept. 1986.
10. Borgeaud, M., R. T. Shin, and J. A. Kong, "Theoretical models for polarimetric radar clutter," *J. Electro. Waves Applic.*, Vol. 1, No. 1, 73–89, 1987.
11. Borgeaud, M., S. V. Nghiem, R. T. Shin, and J. A. Kong, "Theoretical models for polarimetric microwave remote sensing of earth terrain," *J. Electro. Waves Applic.*, Vol. 3, No. 1, 61–81, 1989.
12. Stogryn, A., "Electromagnetic scattering by random dielectric constant fluctuations in a bounded medium," *Radio Science*, Vol. 9, 509–518, 1974.
13. Fung, A., and H. Fung, "Application of first-order renormalization method to scattering from a vegetated-like half space," *IEEE Transactions on Geoscience Electronics*, Vol. 15, 189–195, 1977.
14. de Wolf, D. A., "Electromagnetic reflection from an extended turbulent medium: cumulative forward-scatter single backscatter approximation," *IEEE Trans. Antennas Propagat.*, Vol. AP-19, No. 2, 254–262, Mar. 1971.
15. Rosenbaum, S., and L. W. Bowles, "Clutter return from vegetated areas," *IEEE Trans. Antennas Propagat.*, Vol. AP-22, No. 2, 227–236, Mar. 1974.
16. Tan, H. S., A. K. Fung, and H. Eom, "A second-order renormalization theory for cross-polarized backscatter from a half space random medium," *Radio Science*, Vol. 15, No. 6, 1059–1065, Nov.–Dec. 1980.
17. Chuah, H. T., and H. S. Tan, "A high order renormalization method for radar backscatter from a random medium," *IEEE Trans. Geosci. Remote Sensing*, Vol. 27, No. 1, 79–85, Jan. 1989.
18. Tsang, L., and J. A. Kong, "Application of strong fluctuation random medium theory to scattering from vegetation-like half space," *IEEE Trans. Geosci. Remote Sensing*, Vol. GE-19, No. 1, 62–69, Jan. 1981.

19. Nghiem, S. V., F. C. Lin, J. A. Kong, R. T. Shin, and H. A. Yueh, "Three-layer random medium model for fully polarimetric remote sensing of geophysical media," *Digest of the Progress in Electromagnetics Research Symposium*, 267, Boston, Massachusetts, July 1989.
20. Tsang, L., J. A. Kong, R. W. Newton, "Application of strong fluctuation random medium theory to scattering of electromagnetic waves from a half-space of dielectric mixture," *IEEE Trans. Antennas Propagat.*, Vol. AP-30, No. 2, Mar. 1982.
21. Tsang, L., and J. A. Kong, "Scattering of electromagnetic waves from random media with strong permittivity fluctuations," *Radio Science*, Vol. 16, No. 3, 303-320, May-June 1981.
22. Ryzhov, Y. A., V. V. Tamoikin, and V. I. Tatarskii, "Spatial dispersion of inhomogeneous media," *Soviet Physics JETP*, Vol. 21, 433-438, 1965.
23. Ryzhov, Y. A., and V. V. Tamoikin, "Radiation and propagation of electromagnetic waves in randomly inhomogeneous media," *Radiophys. Quantum Electron.*, Vol. 13 (trans. from Russian), 273-300, 1970.
24. Tamoikin, V. V., "The average field in a medium having strong anisotropic inhomogenieties," *Radiophys. Quantum Electron.*, Vol. 14 (trans. from Russian), 228-233, 1971.
25. Kong, J. A., *Electromagnetic Wave Theory*. New York: Wiley-Interscience, 1986.
26. Chu, N. C., "Phase Fluctuations of Waves Propagating Through a Random Medium," S.M. Thesis, Massachusetts Institute of Technology, June 1990.
27. Chu, N. C., J. A. Kong, H. A. Yueh, S. V. Nghiem, J. G. Fleischman, S. Ayasli, and R. T. Shin, "Covariance of phase fluctuations of waves propagating through a random medium," submitted for publication, 1990.

Nelson C. Chu received the B.S. degree in electrical engineering from the Virginia Polytechnic Institute and State University in 1988. Since 1988 he has been with the Department of Electrical Engineering at the Massachusetts Institute of Technology as a graduate student, and a Research Assistant at the MIT Lincoln Laboratory. He received his S.M. degree from MIT in 1990.

Jin A. Kong is Professor of Electrical Engineering and Chairman of Area IV on Energy and Electromagnetic Systems in the Department of Electrical Engineering and Computer Science at the Massachusetts Institute of Technology in Cambridge, Massachusetts. His research interest is in the field of electromagnetic wave theory and applications. He has published seven books and over 300 refereed journal and conference papers, and is the Editor of the Wiley Series in Remote Sensing, and Chief Editor of the Elsevier book series of Progress In Electromagnetics Research (PIER).

Simon H. Yueh received the SB (1982) and SM (1984) from the Electrical Engineering Department of National Taiwan University, Taiwan, and is currently working on the Ph.D. degree in Electrical Engineering at Massachusetts Institute of Technology, Cambridge. His fields of interest are electromagnetic field theory and remote sensing.

Son V. Nghiem received his B.S. degree (1985) in electrical engineering with Summa Cum Laude Honor from Texas A & M University and his M.S. degree (1988) in electrical engineering and computer science from the Massachusetts Institute of Technology. He is currently working toward his Ph.D. degree and his research interest encompasses electromagnetic wave theory, polarimetric remote sensing, and atmospheric and ionospheric effects on wave propagation. Mr. Nghiem is a member of the IEEE and the Honor Society of Phi Kappa Phi.

Jack G. Fleischman received the Ph.D. degree in physics from the University of Pennsylvania in 1987. His dissertation was in the field of elementary particle physics. Since 1988 he has been a member of the Research Staff in the Systems and Analysis Group at the MIT Lincoln Laboratory. His research activities include polarimetric remote sensing, electromagnetic propagaion and systems analysis. Dr. Fleischman is a member of the American Physical Society, Sigma Pi Sigma and the New York Academy of Sciences.

Serpil Ayasli received the B.S. degree in electrical engineering, and the M.S. and Ph.D. degrees in physics, all from the Middle East Technical University, Ankara, Turkey, in 1973, 1975, and 1978, respectively. From 1975 to 1979 she was a member of the teaching staff at the Department of Physics, Middle East Technical University. In 1979 she started working as a Postdoctoral Fellow at the Center for Theoretical Physics and the Center for Space Research, Massachusetts Institute of Technology, where she pursued research on theoretical modeling of astronomical X-ray burst sources until 1982. Since 1982 she has been with the MIT Lincoln Laboratory. Her current research activities include terrain-specific radar propagation and clutter modeling, radar cross-section evaluation, and ground-based radar performance predictions.

Robert T. Shin received his SB (1977), SM (1980), and Ph.D. (1984) in Electrical Engineering from the Massachusetts Institute of Technology. Since 1984 he has been on the Research Staff in the Air Defense Techniques Group at the MIT Lincoln Laboratory. His research interest is in the areas of electromagnetic wave scattering and propagation and theoretical model development and data interpretation for microwave remote sensing. He is the coauthor of *Theory of Microwave Remote Sensing* (Wiley, 1985). Dr. Shin is a member of the IEEE, American Geophysical Union, Tau Beta Pi, Eta Kappa Nu, and commission F of the International Union of Radio Science.

THEORETICAL MODELING FOR PASSIVE MICROWAVE REMOTE SENSING OF EARTH TERRAIN

by
J. A. Kong
Center for Electromagnetic Theory and Applications
Research Laboratory of Electronics and
Department of Electrical Engineering and Computer Science
Massachusetts Institute of Technology
Cambridge, Massachusetts 02139, USA
TEL: 617-253-5625
FAX: 617-253-0987

Abstract

In this paper we address the issue of theoretical modeling for passive microwave remote sensing of terrain media such as snow, ice, vegetation, and periodic surfaces. Historically, the volume scattering effects stimulated the development of the continuous random medium model and the random discrete scattering model for the description of the media. Theoretical treatments were developed along two different paths. Invoking the principle of reciprocity, the wave theory based on Maxwell's equations has been used to calculate the emissivity. The other approach was to start with the radiative transfer equations and solved for the brightness temperatures directly. Attempts have been made to derive the radiative transfer theory from the wave theory. At the same time, both theoretical approaches have been used to calculate the radiometric emissions and to interpret experimentally measured data.

The successful interpretation of the Cosmos 243 data was perhaps the first most important step towards a serious development of the continuous random medium model to account for the volume scattering effects of snow ice fields. Subsequent interpretation of measurement results from snow field with both passive radiometers and active radar systems established a unique position for its description of earth terrain media. Recent efforts in classifying sea ice with correlation function characterization are demonstration of acceptance of this model. Future inverse scattering developments will perhaps rely heavily on this model.

In this paper, we shall illustrate the development of the theoretical models and present data matching results with measurements made in snow ice fields and vegetation canopies. The emissivity calculations for periodical rough surfaces will also be presented and compared to measured data.

Recent development in polarimetric active remote sensing with synthetic aperture radar has created significant theoretical results and practical applications. In passive remote sensing, the third and the fourth Stokes parameters for earth remote sensing have not received much attention in the past partly due to the expected small values any measurement can yield. We have made initial calculations and experimental measurements to show that at least the third Stokes parameter can give appreciable number in both theoretical prediction and actual experimentation in a plowed field. Such results may have practical implications in measuring wind directions in ocean waves, for instance. We believe polarimetric passive remote sensing is a viable field which should be explored in light of its potential applications that may derived from the full Stokes vector instead of its first two parameters, i.e.,ters, i.e., the horizontally and vertically polarized brightness temperature components.

Acknowledgement: The work presented in this paper contains contributions from L. Tsang, R. Shin, S. Nghiem, H. Yueh, J. Lee, M. Borgeaud, K. O'Neill, M. Veysoglu, H. Han, C. Hsu, and others.